Han Wei

Experimental and Numerical Studies of Burden Layers at Blast Furnace Charging

Åbo Akademi University

Han Wei

Born in 1992, Rizhao, Shandong, China

Previous Studies and Degree

B.Sc. Materials Science and Engineering, 2016
University of Jinan, Shandong, China

Master and Ph.D. study in Materials Science and Engineering from 2016
Shanghai University, Shanghai, China

Experimental and Numerical Studies of Burden Layers at Blast Furnace Charging

Han Wei

Supervisor

Professor Henrik Saxén
Faculty of Science and Engineering
Åbo Akademi University, Finland

Co-supervisor

Docent Mikko Helle
Faculty of Science and Engineering
Åbo Akademi University, Finland

Professor Yaowei Yu
School of Material Science and Engineering
Shanghai University, China

Reviewers

Professor Ari Jokilaakso
School of Chemical Engineering
Aalto University, Finland

Professor Yansong Shen
School of Chemical Engineering
University of New South Wales, Australia

Opponent

Professor Yansong Shen
School of Chemical Engineering
University of New South Wales, Australia

To my family

山止川行

风禾尽起

Preface

The research effort reported in this doctoral dissertation was carried out during the years 2018-2019 at the Metallurgy Engineering Laboratory at Shanghai University, China and the years 2020-2022 at the Process and Systems Engineering Laboratory at Åbo Akademi University, Finland. The Chinese Scholarship Council is gratefully acknowledged for giving me opportunity and financial support to complete this project.

First of all, I would like to express my sincere thanks to my supervisor Prof. Henrik Saxén, for his instructive advice and useful suggestions on each state of the process for this thesis work. It has been a great privilege and joy to study under his guidance and supervision. He is the kindest, most patient and knowledgeable supervisor in my heart. I would like to thank Prof. Yaowei Yu, who gave me large encouragement and confidence to visit Finland and great help for my thesis work.

I am extremely grateful to my colleagues at the laboratory for their help and company. I would like to thanks Weiqiang, Debanga, Meng, Guanwei, Gopala, Javier, Emiliano, etc. Special thanks to Weiqiang for his help for starting my life in Finland and also to Debanga for great discussions and help for my research. Thanks for Alf and Vivéca for their practical help of office affairs. Great thanks to all my friends in Finland for their company and inspiration. It has made my life in Finland full of color and makes me feel at home.

I would like to acknowledge the endless support and understanding of my beloved parents, sister and my boyfriend, Hang Shi. Your listening, encouragement and trust are the biggest motivations for my life and work.

At last, bless myself, forever young, forever weeping and forever on the road!

Turku, Finland, September 2022

Han Wei

Abstract

The blast furnace (BF) is the main production unit in the processing of iron ore to molten iron ("hot metal") in the steelmaking industry. It is a large process with huge throughput and energy consumption, so even a slight improvement of its efficiency can lead to considerable reductions in costs and harmful emissions. The charging system is the only way by which the initial distribution of the raw materials can be controlled. This distribution not only determines the structure of the arising burden bed, but also the chemical and thermal efficiency of the gas. These are crucial factors for achieving a low rate of reductants, a long life length and a more sustainable operation of the furnace.

Focusing on the behavior of particles forming heaps and layers in granular systems, this thesis has studied some questions related to burden-layer formation, burden bed properties, burden descent and gas flow distribution in the blast furnace throat and shaft.

Firstly, the effects of particle shape and physical parameters on the porosity and angle of repose of iron ore particle heaps were simulated by discrete element method (DEM). Models of non-spherical particles (cylinders and cones) were established using the sphere-cluster method. For comparison and model validation, small-scale experiments were undertaken with particles of the same shapes prepared in the laboratory. The consistency of the simulated and experimental results demonstrate that the established DEM model can be used for the prediction of the porosity of a particle system.

Some key physical parameters of the main burden materials (pellets, sinter and coke) were measured and validated by experiments. The experimentally determined parameters were the Young's modulus, Shear modulus, Poisson's ratio, particle density, coefficient of restitution, as well as coefficients of static and rolling friction. The experimental and calculated results were found to exhibit good agreement, which confirmed that the measured DEM parameters were of sufficient accuracy to be used in simulation of the burden distribution and descent in the blast furnace.

DEM models describing the porosity distribution and radial ore-to-coke mass ratio of the burden layers in the blast furnace shaft were successfully established based on a bell-less burden charging system with 2D slot and 3D sector throat models. An experimental bell-less charging system with a scale of 1:10 compared to an industrial BF was designed and operated in a set of experiments. DEM simulations of the corresponding system showed results in general agreement with the empirical findings, validating the numerical models.

Two kinds of non-uniform descent of burden in the upper part of the blast furnace were considered in a numerical DEM-based model, where the descent rate in the furnace center is greater than the descent rate at the wall or vice versa. The results showed that the ore-to-coke ratio decreases where the burden descent rate is low and increases where the descent rate is high.

Finally, the effect of intermittent charging on the thermal and flow conditions in the upper shaft was analyzed by Computational Fluid Dynamics (CFD)

combined with DEM. A model of the counter-current flow of gas and solids and the temperature of the two phases in a simplified setup was developed. The results clarified how the temperature and velocity of the ascending gas are affected by the intermittent charging.

Sammanfattning

Masugnen är den huvudsakliga processenheten vid produktion av råjärn för stålframställning. Den är en industriell reaktor med mycket stor genomströmning av material. Ugnen har en hög energiförbrukning, vilket innebär att redan små relativa förbättringar i driften kan har stora implikationer för material- och energiåtgång samt för de utsläpp som förorsakas av processen. Masugnens chargering, d.v.s. inmatningen av det fasta råmaterialet vid toppen, är av stor betydelse för styrningen av råmaterialets radiella fördelning i ugnens övre del. Chargeringen bestämmer beskickningens struktur i masugnsschaktet, vilket påverkar ugnens termiska och kemiska verkningsgrad. Dessa faktorer är centrala för att uppnå driftpunkter med låg förbrukning av reduktionsmedel, lång ugnskampanj samt en hållbar järnframställning.

Föreliggande avhandling studerar beteendet hos partiklar som bildar högar och lager i granulära system. Avhandlingen behandlar frågor av speciell relevans för bäddens egenskaper i masugnsschaktet, där lager av olika beskickningsmaterial bildas vid chargeringen och efter det långsamt sjunker nedåt i ugnen. För att beskriva hur gasen fördelas i schaktet måste även porositeten hos materialbädden vara känd.

I den första delen av arbetet studerades inverkan av partikelform och fysikaliska parametrar på porositeten och rasvinkeln för högar av järnbärare. Systemet simulerades med diskreta element-metoden (DEM), där partiklar med annan form är sfärisk skapades genom att klumpa ihop överlappande sfärer (eng. sphere-cluster). För jämförelse och för validering av den matematiska modellen utfördes småskaliga laboratorie-experiment med partiklar av samma typ. Överensstämmelsen mellan de simulerade och experimentella resultaten visade att DEM-modellen kan användas för att prediktera porositeten hos partikelsystemet.

Några viktiga fysikaliska parametrar hos de huvudsakliga beskickningsmaterialen (pelletar, sinter och koks) uppmättes och validerades med hjälp av experiment. De parametrar som bestämdes experimentellt var elasticitetsmodulen, skjuvmodulen Poissons konstant, partikeldensitet, restitutionskoefficienter, samt statiska och rullnings-friktionskoefficienter. De experimentella och simulerade resultaten befanns överensstämma väl, vilket bekräftade att DEM-parametrarna som bestämts var tillräckligt noggranna för att kunna utnyttjas vid simulering av beskickningsfördelning och -sjunkning i masugnen.

DEM-modeller som beskriver bäddporositetens och den radiella malm-koks-fördelningen hos beskickningen i masugnsschaktet skapades för ett system med s.k. Paul Wurth-chargeringsmål med två- eller tredimensionella modeller för masugnens gikt. Ett experimentellt klocklöst (eng. bell-less) uppsättningsmål i laboratorieskala i 1:10-skala jämfört med en industriell ugn byggdes och utnyttjades i experiment. DEM-simuleringar av motsvarande system gav resultat som generellt överensstämde med de experimentella resultaten, vilket validerade de matematiska modellerna.

Två typer av ojämn sjunkning av beskickningen i schaktet studerades även numeriskt med hjälp av en DEM-modell, där bädden simulerades sjunka snabbare eller långsammare i masugnens centrala del. Resultaten visade att malm/koks-förhållandet avtar i regioner där bädden sjunker långsamt, medan kvoten ökar i regioner där sjunkhastigheten är hög.

I arbetets sista del studerades hur en satsvis chargering påverkar det termiska och flödesmässiga dynamiska tillståndet hos den översta delen av masugnsschaktet med hjälp av flödessimulering (eng. Computational Fluid Dynamics, CFD) kombinerad med DEM, s.k. CFD-DEM-teknik. En förenklad och nerskalad modell utvecklades, som beskriver motströmsflödet av gas och beskickningsmaterial och temperaturerna hos de två faserna. Modellen klargjorde hur temperaturerna och gashastigheten påverkades av den oregelbundna chargeringen, vilket förklarar fenomen som man kan observera vid ugnstoppen i den verkliga driften av masugn.

List of publications and contribution of the author

The thesis consists of a summary and the following five journal publications.

I.   H. Wei, X.J. Tang, Y. Ge, M. Li, H. Saxén, and Y.W. Yu, "Numerical and experimental studies of the effect of iron ore particle shape on repose angle and porosity of a heap", Powder Technology, 353 (2019) 526-534.

II.   H. Wei, H. Nie, M. Li, Y. Li, Y. Ge, L. Zan, H. Saxén, Y.W. Yu, "Measurement and simulation validation of DEM parameters of pellet, sinter and coke particles", Powder Technology, 364 (2020) 593-603.

III.   H. Wei, W.T. Ding, Y. Li, H. Nie, H. Saxén, Y.W. Yu, "Porosity distribution in blast furnace throat during the charging process ", Granular Matter, 23 (2021) 1-12.

IV.   H. Wei, D. Mondal, H. Saxén, Y.W. Yu, "Numerical investigation of the radial ore-to-coke ratio in the blast furnace throat during non-uniform burden descent", major revision to Steel Research International, September, 2022.

V.   D. Mondal, H. Wei, Y.W. Yu, H. Saxén, "Computational study of gas-flow and temperature dynamics at blast furnace charging", Steel Research International, 2022, 2200035. https://doi.org/10.1002/srin.202200035

The author of this thesis is the main author of Papers I to IV. The author conducted all the experimental parts at the Metallurgical Engineering Laboratory in Shanghai University, China and all the DEM simulation parts, including the establishment of the two-dimensional and three-dimensional DEM models. The experimental devices in Papers I, II and III were designed and made with the help of the co-authors. The author wrote the first manuscripts of the Papers I to IV and revised the papers together with Prof. Saxén and Prof. Yu. In Paper V, Mondal was responsible for the main work and writing of the first draft. The present author contributed to the DEM model design and some data analysis.

Table of contents

1 Introduction

Nowadays, reducing the emissions of CO_2 in industrial processes is a hot topic which has attracted extensive attention. The steel industry is facing large restructuring in the future as it today contributes by 7-9% of the global anthropogenic CO_2 emissions: in particular, the blast furnace (BF) process produces almost 70% of the total CO_2 emissions from the steelmaking industry [1]. The Net Emissions by 2050 Scenario (NZE) proposed by International Energy Agency (IEA) shows a pathway and goal (Figure 1) for the global energy sector to achieve net zero CO_2 emissions by 2050. However, the crude steel production shows no trend of decrease. In contrast, the request of reducing the CO_2 is emergent. The direct CO_2 intensity of crude steel production has been relatively constant in the past few years. Achieving this reduction and maintaining it after 2030 will not be easy. All the same, iron and steel industry play an important role in green economy as the sectors and technologies. The clean energy, wind energy, low-carbon transport and light vehicles, fuel-efficient infrastructure and recycling facilities are all dependent on steel products. Furthermore, steel can be used as a recycling material.
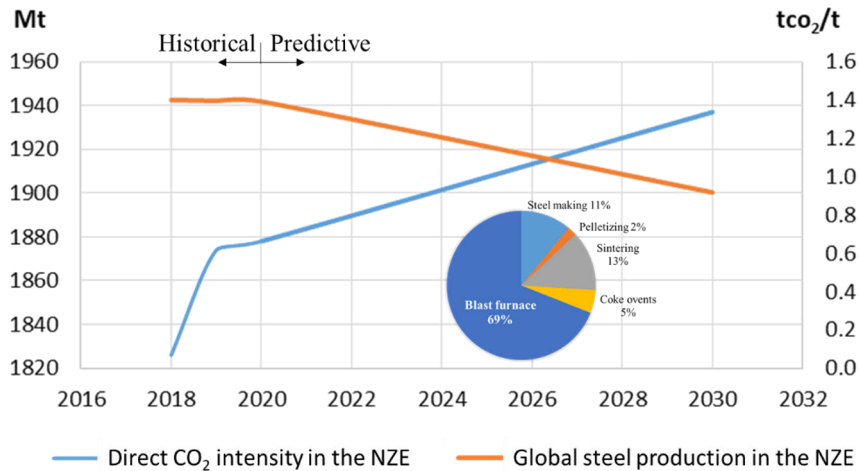

Figure 1. *Historical and predictive value of global steel production and direct CO_2 intensity in the NZE (IEA). The inserted figure is the CO_2 emissions in steelmaking [1].*

The BF is one of the principal ironmaking units in the world for providing liquid iron for steelmaking. Over the years, the volume of the blast furnace has been frequently enlarged and the largest furnace has today an inner volume over 5000 m^3 [2]. This process is a counter-current unit which is operated at high temperatures. Ferrous oxides are charged at the top and the reducing gas is generated in the lower part as a result of reaction between coke, injected coal and preheated combustion air (called blast). The solid raw materials are charged in alternate layers of coke and ferrous oxides to ensure good permeability when the oxides start melting in the lower part of the furnace. The reducing gas from the combustion zone, raceways, flows rapidly upwards, meeting the slowly descending layered burden. As about 70% of the energy

demand of steelmaking is required in the blast furnace, it is obvious that the efficiency of the BF is of crucial importance for the whole steelmaking chain [3]. Therefore, it is imperative that the BF be efficiently operated and that major upsets in the operation be avoided.

In the long run the existing coal-based reduction processes must be replaced by new production concepts based on recycled raw materials and renewable energy. However, in the short term, accelerated efforts must be made to improve the existing unit processes in order to increase material efficiency and decrease harmful emissions. To make full use of energy and reduce the emissions, the furnace should be operated at a high production with low reductant rate. It is a great challenge to achieve and maintain this state.

The charging system can control the initial distribution of raw materials in blast furnace, which has a major impact on the operation of the upper part of the blast furnace [4]. Since coke has larger size and smaller density than sinter and pellets and that the void fraction within the coke layer is higher, the coke layers are more permeable to gas flow and the radial distribution of the ore-to-coke ratio will therefore directly affect the gas flow distribution in the shaft. Another factor that also affects the gas flow distribution is the bed voidage distribution, which depends on the particle sizes and whether small and large particles are mixed or not. The ore-to-coke distribution also strongly affects the thermal conditions, due to the heat capacity of ore is about four times higher than that of coke, which means that a larger share of ore yields slower heating during burden descent, and the gas is correspondingly cooled more during its ascent. Finally, as coke is the only solid phase that exists below the melting line of the ores, the coke layers will act as gas distributors in the cohesive zone between the impermeable softening and melting ore layers: this also affects the conditions in the lumpy zone.

Based on the above, it can be concluded that understanding the influence of the burden distribution, radial ore-to-coke ratio and gas flow during burden charging and descent is a necessary prerequisite for developing appropriate strategies for controlling the blast furnace upper operation. This thesis is focused on the properties of burden layers in the upper shaft of the blast furnace with a bell-less charging system using simulation methods combined with small scale laboratory experiments. Computational Fluid Dynamics (CFD) is used for the simulation of gas flow and heat transfer in blast furnace, while the Discrete Element Method (DEM) is used for the simulation of particulate flow. Since the burden bed can be seen as a series of granular heaps, research on the properties of a heap of granular matter is helpful for the understanding the behavior of burden in the blast furnace shaft. Therefore, the thesis started by discrete element modelling of particle heaps. Since the results of DEM–based analysis crucially depend on the model parameters, efforts were made to estimate the DEM parameters of commonly used burden materials. Based on this, DEM models of the burden charging and descent and a CFD-DEM model of the gas-solid thermal and flow conditions in the upper shaft were established. Some of the findings of the models have been validated by small scale experiments carried out in the laboratory and also by using observations about e.g. burden distribution from excavated quenched industrial blast furnaces.

This thesis is built up from six chapters. The first chapter gives a short review of the research background and the subject of the work. The second chapter introduces the scientific questions in the field of granular system and goes into more detail on ironmaking, in particular the burden charging in the top of the BF.

Chapter 3 gives a literature review about the research methods and properties of particle packing. The development of the modelling of BF burden and gas flow and the principles of DEM are well concluded.

For the chapter 4, the research contents of this work is discussed in detail. It starts from the basically research of the properties of a heap and the calibration of the DEM parameters of the main burden materials, which are all essential to the BF charging simulation. Based on these, the development of the models and the results of burden and gas flow distribution at the upper part of the shaft are discussed. Chapter 5 and 6 finally present the main conclusions and recommendations for the future work.

2 Granular system and blast furnace

2.1 Granular system

Granular materials are thought to be the second most abundant material on earth after fluids [5]. Granular systems (Figure 2), from small nanoparticles to sand, powders and foams are ubiquitous in daily life and in industrial and geotechnical applications [6], such as sandpiles in the desert, grain heap in agriculture, capsule formation in pharmaceutical processes, sintering and pelletizing in metallurgical processes, and burden flow and descent in the blast furnace process. A granular material is, in fact, a cluster of distinct particles that lose energy when interacting with other particles [7], which have properties that are different from those commonly associated with either solids, liquids, or gases. Therefore, the mechanical properties of granular matter, including static packing, rheology and stability, are still poorly understood. In 2005, the "Science" journal listed the non-equilibrium dynamics theory of particulate matter as one of the 125 major scientific problems to be solved urgently.

Figure 2. *Granular system (from Wikipedia Commons).*

In general, a granular system is opaque. Particles in the granular system are discrete and the dissipative interaction between them increases the complexity of the bulk behavior, which brings much difficulties to the research on such systems. The particles maintain their solid state under the action of gravity, and once subjected to small external perturbations, they will show structural relaxation and exhibit the characteristics of a fluid [8]. A test for the fluidity of a granular system is shown in Figure 3: a material in a heap remains at rest even though gravitational forces create macroscopic stresses on its surface. As the slope is increased slightly, grains start to flow, but the flow is clearly not that of an ordinary fluid because it only occurs in a boundary layer at the heap surface with no movement in the bulk of the heap. Thus, although individual grains are solid, it is inappropriate to classify their collective properties as entirely solid-like or liquid-like [5].
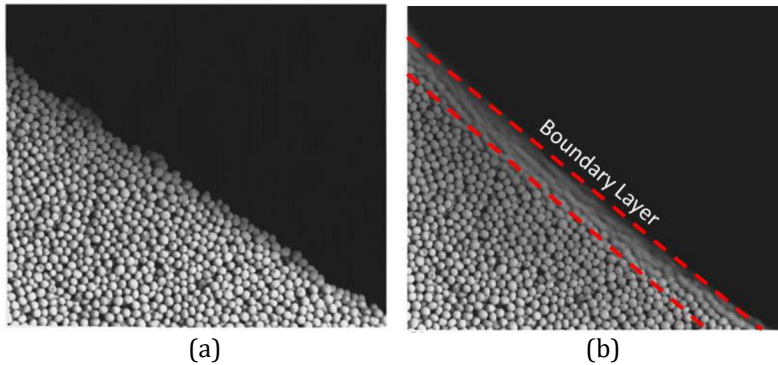
Figure 3. *Sandpile at rest with a slope smaller (a) and larger (b) than the angle of repose. The same heap after the slope has been increased slightly to create an avalanche.*

Properties of granular heap can be divided into two categories according to the research scale: macroscopic and microscopic [9]. The former includes angle of repose [10], slope angle, stress distribution [10, 11], pressure distribution and particle density [12, 13], while the latter refers to particle properties, such as coefficient of rolling friction [14], coefficient of static friction [15], Poisson's ratio, coefficient of restitution and Young's modulus. Although there are many studies on the macroscale properties of granular systems, only a few investigations have probed the structure and dynamics of granular systems at the particle level and in three dimensions, owing to the experimental difficulty of determining the position and orientation of individual particles [16]. Because of this, many modern techniques have been introduced into the particle research. For example, magnetic resonance imaging, X-ray tomography and high-speed video have been applied to realize 3D-particle tracking. Such kinds of experiment are one of the most direct and trustworthy ways to study behavior of granular matter even though they usually come at a high cost. In recent years, with the development of the computer technology and the improvement of computing speed, numerical simulations, including Monte Carlo (MC), cellular automaton (CA) and discrete element method (DEM), have been used to study many aspects of granular flow which are hard to observe in experiments.

Research on the granular system is the foundation to many improvements and innovations in transportation and storage of industrial raw materials. A better understanding of granular systems is useful for designing and optimizing many industrial processes. For example, in the concrete and ceramic industries, optimizing the particle packing is important for enhancing the performance of concrete and ceramic materials. In the pharmaceutical industry, the packing structure of particles is related to the flowability, which impacts the compaction process, ultimately influencing the quality of the tablets. In blast furnace ironmaking, the porosity of burden bed has a considerable effect on the gas distribution and chemical reactions between raw materials (bulk particles) and the gas. It also influences the thermal behavior in the furnace. Therefore, further understanding of the behavior of granular media can yield better process design and operation on industrial processes, which can have a profound impact on product quality as well as materials and energy efficiency.

2.2 Blast furnace ironmaking

The blast furnace is a huge reactor with the biggest hearth diameter between 14 and 15 m [17], which is a main ironmaking unit in the steel industry. The BF is a high-temperature moving bed reactor involving counter-, co-, and cross-current flows of gas, liquid, solid, and powder, coupled with heat and mass transfer and chemical reactions. The BF produces molten iron, called "pig iron", by the reducing action of carbon (mainly from coke) or hydrogen at very high temperature in the presence of a fluxing agent such as limestone. Figure 4 shows a schematic of a BF with a top burden charging system [18]. The BF ironmaking process can be simply described as follows:

Solid iron oxides (in the form of pellets, sinter or lump ore), coke and limestone, are charged in layers using either a bell or bell-less charging system at the top of the furnace, and as the burden descends in the furnace it is heated up by the ascending gas. The gas is generated by injecting oxygen-enriched hot air, called blast, which is blown into the furnace through the nozzles, tuyeres, at the lower part, forming void combustion zones known as raceways. Coke reacts with oxygen to form the reduction gas, mainly carbon monoxide, and part of the heat required in the process is released in this partial combustion process. As the reduction gas rises through the furnace it reacts with the descending oxides, reducing them, creating metallic iron and carbon dioxide. The iron melts in the lower part of the process together with the gangue and coke as, which form slag, and the molten products are tapped from the bottom of the furnace through tapholes drilled in the sidewall. The gas leaves the furnace at quite low temperature (100-150 °C) at the top.

During the above process, the physical state of the materials varies because of the temperature distribution from the bottom to the top of the blast furnace, which can be mainly divided into three zones: lumpy zone, cohesive zone and dripping zone. The lumpy zone is the area where the burden exists in solid form and usually occupies the middle and upper part of the furnace shaft. The blast enters through the tuyeres preheated to temperatures from 1000 °C to 1250 °C often together with an auxiliary reductant, such as pulverized coal or natural gas to reduce the requirements of the more expensive coke. The tuyeres are uniformly located around the circumference of the furnace near the top of its lowest part, the hearth. The flame that is formed in the raceways where the oxygen reacts with the coke and injected reductant has a temperature in excess of 2000 °C. The charged material at the top slowly heats up and at a temperature about 1100 °C the ore starts softening and melting. The cohesive zone in the furnace is the zone where the softening and melting take place to form liquid slag and iron, and here the permeability of the ore layers decreases and these layers become nearly impermeable. As the ore melts, only coke remains solid below the cohesive zone and this coke bed structurally supports the cohesive and lumpy zones. The liquids below the cohesive zone percolate through the coke bed in the form of droplets/rivulets in the dripping zone to the hearth, from where they are periodically drained out through a taphole. The main components of the pig iron are metallic iron (94-95 %), dissolved carbon (4-4.5 %) as well as some impurities which are the result of reduction reaction of oxides, such as silicon,

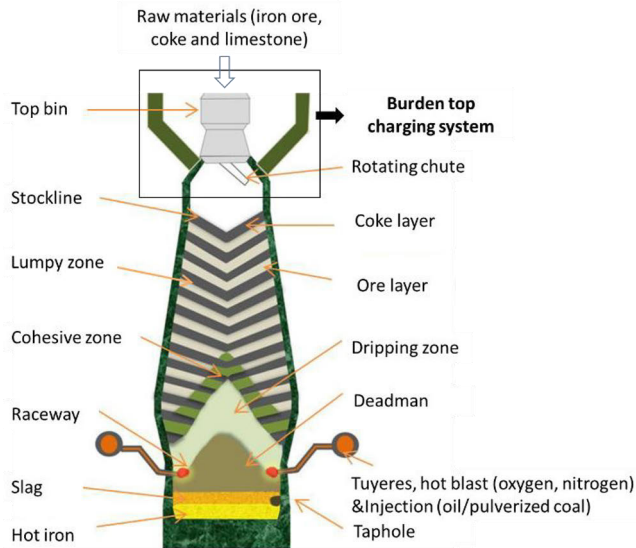manganese, titanium, sulphur or phosphorus. Slag is formed by unreduced oxides from the ore and fluxes.

Figure 4. *Schematic of a typical ironmaking BF and its different zones and of alternate coke and ore burden layers [18].*

The blast furnace operation scheme refers to the collection or series of rules and means adopted by blast furnace operators under certain smelting conditions in order to achieve a high production rate and product quality, low coke consumption, high yield and long campaign life of the blast furnace. To achieve a smooth and efficient operation of the BF, four main control schemes often applied: burden distribution scheme, slag forming scheme, blast scheme and thermal scheme [4].

(1) Burden distribution (charging) scheme is the general term of the way of charging the solid raw materials into the furnace, which specifically refers to the charging sequence, the chute (or movable armour) setting, batch weight and the stockline level when charging into the furnace.

(2) Blast scheme refers to various control parameters for blowing into the furnace through the tuyeres under certain smelting conditions (i.e. the quantity and quality of air blown into the furnace and the air inlet state of the tuyere).

(3) Slag forming scheme refers to controlling various physical and chemical properties of slag, such as melting point and liquidity so it can be separated from the hot metal. The physical characteristics of slag are affected by the ratio and distribution of the raw materials.

(4) The thermal system refers to the thermal state of the furnace, which mainly concerns hearth temperature according to the smelting conditions and desired hot metal characteristics. The thermal system is essentially the comprehensive collection of various operating actions. It is mainly adjusted based on blast control.

Figure 5 shows the driving forces of a blast furnace that cause the burden to descent. The gravity of burden particles and the reduction/melting of the iron

base to produce pig iron drive the continuous descent of the upper charge. The coke combustion in front of the tuyeres provides 35-40% space, the gasification of coke by the direct reduction reactions provides 15% space, the ore compression and melting provide 30% space, and the discharge of iron and slag provides the remaining percent [17]. Regarding the reasons for the descent of upper charge, coke combustion plays a key role.
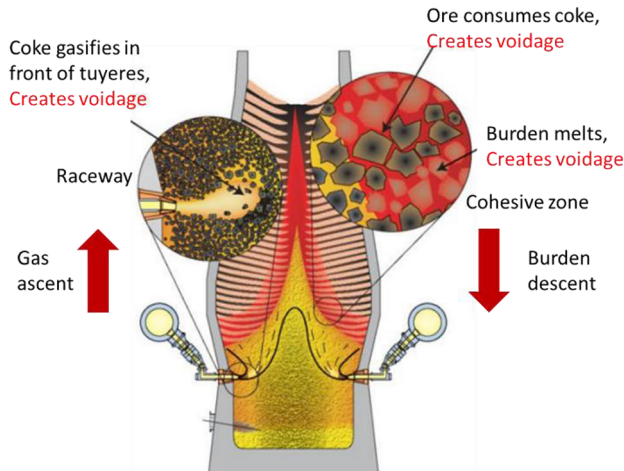

Figure 5. *Driving forces of a blast furnace: the counter–current process creates voidage at the indicated areas causing the burden to descend [17].*

In the BF, the voidage or a permeability index is usually used to express the permeability of blast furnace charge. The distribution of the burden, in the upper part of the BF plays an important role for the permeability of the shaft, which affects the gas distribution, and through it heat and mass transfer and the indirect reduction of the iron ore. Therefore, it is very important to control the voidage or permeability of the bed in the shaft.

To achieve this, the degree of interaction of the solid and gas can be affected by the "top adjustment", which is the only way to control the initial distribution of raw materials through changing the charging program. Today, most furnaces apply bell-less charging systems which give the operators good opportunities to control the formation of the burden layers. It is therefore clear that knowledge about how the burden particles are distributed at charging and during burden descent is useful for designing operation and control strategies and for troubleshooting in the daily operation.

"Lower adjustment" refers to how to control the furnace state by changing the air supply system, i.e., to control the combustion zone and the initial distribution of gas by changing the blast and injection parameters appropriately. Combining the two adjustment methods is the key to control the smooth operation of the furnace, to obtain a reasonable distribution of the gas and to achieve or maintain a high utilization degree of the gas. Generally speaking, the effect of lower adjustment is faster than that of upper adjustment, but the former offers less means to control the radial distribution of the gas.

2.3 Blast furnace charging system and burden distribution

The burden distribution scheme, which determines the distribution of raw material, the particle segregation and the ore-to-coke ratio, has a direct impact on the top gas and temperature distribution, the structure of the cohesive zone, the thermal state and the chemical reactions of the blast furnace. The charging equipment, charging method and the properties of burden materials all play important roles in achieving a desired distribution of voidage and particle size of charged materials in the furnace. Therefore, the conceptual framework of the burden distribution is rather complex. This subsection part will introduce the development of charging equipment, the original charging materials and effects of burden charging on burden distribution and thus gas distribution.

2.3.1 Development of the charging equipment

Blast furnace charging refers to how to transfer the burden materials through the locks in the furnace to desired locations on the burden surface in the BF throat. In the development of the blast furnace, the most commonly used top charging system can be divided into two kinds according to whether there is what is called a bell: bell top and bell-less top (Figure 6). The former includes either a single bell or two bells.
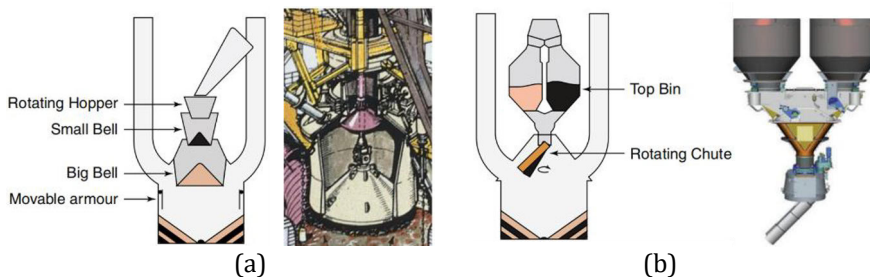

Figure 6. *Blast furnace charging system of bell top (a) and bell-less top (b)[17]. Pictures taken from company websites.*

The bell top charging equipment with two bells (small bell and large bell), also called "McKee Top", was first designed by the American McKee company in 1907. Until 1980s, the McKee top was the most widely used charging equipment in the world. The working principle (cf. Figure 6a) is that the bell blocks the opening of the hopper when it is raised and the burden materials will fall into the throat once the bell is lowered. Compared with single bell, two bells can overcome the shortage of loss of gas, since the upper bell is closed when the lower opens. However, this method still has the problem of non-uniform burden distribution, and most of the raw materials are charged to the wall position. To partly address this weakness, this charging system is often equipped with a movable throat armour to gain some control over the burden distribution of the charged materials (cf. Figure 6a) [17]. The sealing ability can only be used fully on low-pressure blast furnaces; if the furnace top pressure is high, the bell leaks easily. In addition, the bell wears out relatively rapidly and needs to be changed. With the growth in furnace volume, an increased demand for more precise burden

distribution and flexibility led to the development and adoption of the bell-less charging equipment.

The bell-less top was firstly designed by Paul Wurth and successfully used in Hamborn steel company in 1972. Therefore, the system is often called "Paul Wurt Bell-less Top". Since then, the bell-less top charging system has become increasingly popular. Compared with the traditional bell top, the greatest advantage of this kind of charging equipment is its flexibility. The bell-less top with a rotating chute, which rotates about the axis of symmetry, can control the angle (burden location) and rings (burden quantity) to realize a desired and more accurate burden distribution. The use of top and bottom sealing valves equipped with rubber sealing rings with good elasticity realizes a separation of the discharge and sealing functions. Therefore, the sealing ability is improved and the equipment can stand high pressure operation and maintain the furnace top pressure. However, this charging system also has its limitations, such as a non-uniform burden distribution and particle segregation [19, 20] across the throat cross-section, particularly for the bell-less top with (early) parallel bin type. The serial bin type can solve the segregation problem, but can only be applied if the smelting intensity is low or moderate.

In a bell-less top, the possibility exists to distribute the fines in the burden over various points of impact by moving the chute to different positions. Coke can be brought to the center by programming of the charging cycle, which is essential to improve the operational stability and efficiency to better hot metal chemistry control. It also contributes to a longer campaign life. With a two-bell charging system, there is less possibility to vary the points of impact and fines will be concentrated in narrower rings. Another problem with bell-top charging is that the dump size is big, which may cause severe shifting of the burden after it has been charged (e.g., "coke push"), which may be difficult to control. In general, the development of the charging equipment has generally been in the direction of achieving a better sealing and more uniform and well-controlled burden distribution.

In addition to the above main charging systems, there are also further improved designs. For example the Gimbal charging system [21], which was designed by Siemens VAI in 2003, is a new type of charging equipment which utilizes a conical distribution chute, supported by rings to produce independent and combined tilting of the chute axis. However, the added flexibility comes with added complexity of the charging programs, which may be an obstacle for an adoption of the technology.

2.3.2 Properties of charging materials

The main burden materials in the blast furnace are of two types: raw materials containing iron oxides and materials containing carbon. The former includes sinter, pellets and lump ore and the latter mainly refers to coke (Figure 7). Sinter and pellets are often used in combination with lump ore as the iron-bearing burden. Lump ore is cheaper than pellets but it has worse properties for the blast furnace. For reaching a high productivity and low coke rate, the maximum lump ore rate is 10-15% [17]. Pellets and sinter are two materials, which are currently used much more widely as the predominant sources of oxides. In general, the

size of lump ore (6-40 mm) is the largest and the size of pellets (11±2 mm) is the smallest. The size of the coke particles (45-60 mm) is much larger than that of the ore and it makes the basic source of energy and acts as a carbon reductant. The properties of burden materials, for example the size range, strength and repose angle, also influence the burden distribution during burden charging.

| Pellets | Sinter | Coke |
| 11 mm (± 2 mm) | 90 % < 25 mm | 25-40 mm |

Figure 7. *Blast furnace materials and the size of them: pellets, sinter and coke.*

Particle mass and size segregation in the furnace shaft lead to poor and uneven bed permeability [22-24]. The permeability of the bed is decreased with an increase in the range of sizes of the raw materials in general and in particular for increased share of fines in the charge (Figure 8). The fines are usually defined as the fraction of the material that is smaller than 5 mm or 6 mm. Most of the fines come from the sinter and lump ore particles. They are also generated by low-temperature reduction–disintegration. Therefore, the strength of the ore materials is very important for a proper burden distribution.
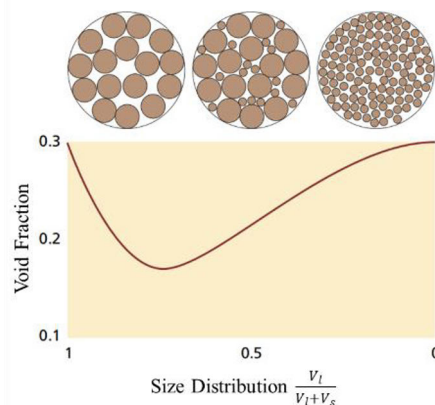

Figure 8. *Void fraction of a mixture of two sizes of spherical particles: large (V_l) and small (V_s). x–axis gives the fraction of the large particles: $V_l / (V_l + V_s)$ [17].*

Particle size segregation occurs when particles move on the chute, because small particles will pass through the voids of large particles and migrate to the bottom close to the chute wall. In addition, when particles flow out of the chute, large particles in the upper part of the chute will preferentially fall on the outer slope of the burden heap while small particles will fall on the inner slope because their kinetic energy is smaller. Furthermore, small particles tend to accumulate close to the point of impact as they are trapped in the voids between the larger ones. The increase of the particle size ratio strengthens the percolation effect

among different-sized particles, especially for mixed layers (where iron-bearing burden components are charged on a coke layer).

Figure 9 shows the angle of repose of blast furnace materials. The angle of repose of a material is dependent on the size distribution [25, 26], shape [27] and moisture content. The angle of repose of coke is larger than that of the ore, which causes ore particles charged on coke to spread from the impact point. Hence, the pellets have the tendency to slide and roll towards the furnace center after charging.
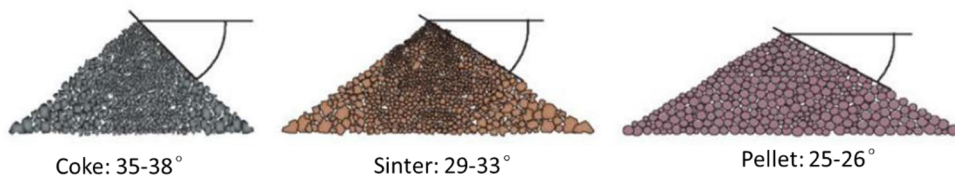

Figure 9. Angle of repose and size segregation of blast furnace materials [17].

2.3.3 Burden distribution

The distribution of the burden, i.e., the charged lump material mainly consisting of preprocessed ore and coke, in the upper part of the BF plays an important role for the efficiency of the BF since it affects the gas distribution, and therefore the heat and mass transfer and indirect reduction of the iron ore. The burden distribution is the consequence of the interaction of properties of the burden materials with the charging mechanism, which is a result of a complex operation.

There are two basic types of gas distribution, namely "central working" and "wall-working" furnaces (Figure 10), which can be realized by the control of the burden distribution. For the former one, the gas flow is directed towards the center. In this case, coke and large ore particles gather at the center of the furnace resulting in the most permeable area in the furnace. For the latter case, smaller coke or ore is charged in the center of the furnace, gas flow is directed outward towards the wall area. The "central working" furnace is more widely used in current blast furnace operation practice, because it can, if provide a stable process and high productivity, good hot metal quality and low reductant rate. The drawback is the sensitivity to burden segregation and the challenge of keeping the width of the central "chimney" restricted: a too strong gas flow in the center lowers the top gas utilization degree and may elevate the top gas temperature, which means that chemical and thermal energy are lost. The "wall working" furnace is less sensitive to inconsistencies in the burden distribution, but the heat loss and refractory wear are larger, and the potential of damaging the refractory or cooling staves or plates in the shaft is higher.

In the bell-less top charging system, the burden distribution in the cross section of the throat can be more easily and accurately controlled. The control of the radial ore-to-coke ratio or the thickness of the ore and coke layers is crucial for a proper burden distribution. The burden distribution influences the shaft conditions in different ways. Since coke particles are larger than ore particles, the coke layers are more permeable to gas flow and the radial distribution or the ore-to-coke ratio will therefore directly affect the gas flow distribution in the

shaft. In addition, the mixed layers have a different permeability and can give rise to circumferential process asymmetry. The blast furnace operator wants permeable (i.e., thick) coke layers and good melting properties of the (i.e., thin) ore layers. However, the overall goal is to reduce or keep the coke rate low, which is contrary to the above aims.
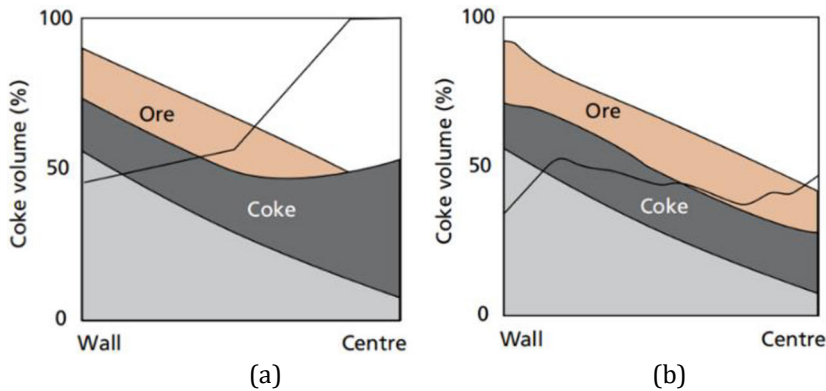

Figure 10. *Burden distribution and the coke volume for the "central working" (a) and "wall- working" furnaces (b) [17].*

An "ideal burden distribution" is achieved with an appropriate charging program, a narrow size distribution and a good strength of the burden material. The charging program allows for some flexibility in building the layers. For example, studies have been conducted on how to charge nut coke (under-sieve small coke) within iron burden layers [28, 29]. This charging mode demonstrated a positive impact on the iron-layer permeability, reducibility, and reducing gas efficiency. Another means is to create program yielding a horizontal burden profile, and an ore-free center with coarse coke. This minimizes the influence of segregation on the charge distribution and allows the gas to distribute through the coke layers from the center to the wall. Charging coarse particles in the center also guarantees a supply of unreacted coke to the hearth, which improves the permeability to liquid flow in the region.

3 Literature summary

3.1 Study on macro- and microscopic granular system

3.1.1 Modelling of particle packing

Particle packing is the process where smaller particles occupy the voids between the larger ones. The small particles in turn contain smaller voids, which are filled with smaller particles and so on (cf. Figure 11, [30]). Packing of granular matter is relevant in many areas and can be divided into two main categories, macroscopic and microscopic, which were introduced in subsection 2.1.
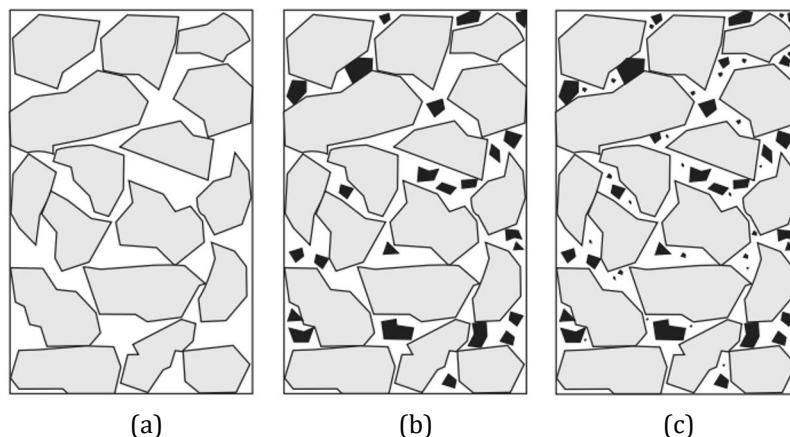

| (a) | (b) | (c) |

Figure 11. *Concept of particle packing. From a to c, smaller particles gradually fill the voids of larger particles.*

A lot of research has been done for the granular heap. However, due to the complexity of the heap structure and the opaque characteristics and complex behavior in three dimensions, it is difficult to understand heap formation and properties merely by laboratory experiments [31-34]. Monte Carlo algorithms have extensively been used by scientists to study the behavior, but the algorithms are based on many assumptions about particle motion and stability criteria which may not reflect the physical truth [35, 36]. DEM has become an option for scientists and engineers to validate and optimize the design of granular material handling system [37, 38].

Early studies mainly focused on spheres or discs in DEM, because mathematical models of sphere-sphere and sphere-wall interactions are well-known [39-41] and a lower computing effort is needed for discs or spheres [42]. However, actual particles in daily life are usually non-spherical and of more complex shape. Therefore, including a description of non-spherical particles in DEM is highly relevant and it is necessary to study properties of non-spherical particles in granular heaps. Researchers have therefore used ellipsoid, super-quadrics [43], polygons and multi-sphere clusters. For example, Gan et al. [13] and Deng and Davé et al. [44] studied the coordination number and radial distribution in heaps of ellipsoids with different sizes and aspect ratios. Höhner et al. [42, 45-47] investigated the movement of ellipsoidal, super-quadric,

polygonal and cylindrical particles in heaps. The advantages and disadvantages of different DEM particle models are listed in Table 1. In particular, multi-sphere approach is today the most common used method due to the gain in flexibility in the shape approximation. The element spheres can be overlapped and the internal contacts are ignored, so that the clump behaves as a rigid body [48] but still uses the contact detection algorithm of sphere modeling. Theoretically, any particle shape can be modelled, although highly angular particles require a large number of small spheres to approximate their sharp edges, making this method unsuitable.

Table 1 *Particle models in DEM simulation.*

Model	Shape	Advantages	Disadvantages
Sphere		*Simple collision model, efficient calculation and lowest computing effort.*	*Unable to express the actual particle shape.*
Ellipsoid /Super-quadrics		*Effective superquadric function, higher accuracy.*	*Iteratively solving non-linear equations, time-consuming, symmetric and convex particles.*
Polygon		*Approximate arbitrarily shaped objects with sharp-edges.*	*Time-consuming, high requirements for computer and very memory consumptive.*
Multi-sphere Clusters		*Simple collision model, a rigid whole with various complex and non-symmetrical particles, relatively faster calculation speed.*	*Complex generation process of particle model, lack generality and limited validity.*

In order to express the shape of particles quantitatively, researchers often use sphericity (φ) or aspect ratio. The former is the ratio of the surface area of a sphere with the same volume as the particle to the surface area of the particle [49]. It can be calculated by Equation 1, where V_p is the volume of the particle and A_p is the particle surface area. The aspect ratio refers to the ratio of width to the height of a particle. Obviously, the sphericity and aspect ratio of spheres are both unity.

$$\varphi = \frac{\pi^{\frac{1}{3}}(6V_p)^{\frac{2}{3}}}{A_p} \tag{1}$$

3.1.2 Properties of granular system

The micro parameters have a deep influence on the macro properties of granular matter, and macro-accurate predictions can be made computationally if the model parameters are carefully selected [9]. These issues have long been a hot topic in research due to the ever-increasing need to understand the behavior of granular system. For example, porosity or void fraction (ε) and packing density (=1- ε) of the particle bed are important aspects in the fields of chemistry, materials and energy engineering.

The porosity distribution of a granular system, such as in a container, a packed bed or a heap, is an important parameter reflecting the internal structure difference caused by the particle itself and the environment. Like for the research on many other properties of granular system, the porosity distribution can be estimated by experimental methods, mathematical expressions and numerical simulation. Recently, Khalili et al. [50] used X-ray computed tomography to explore the porosity-depth variation below a porous media interface of multi-sized spherical or arbitrarily-shaped granules. Some researchers focused on the distribution of porosity in containers. Yu and Standish [51] developed a mathematical packing model from the viewpoint of the microstructure of particles to predict porosity of packed beds. Mueller [52] proposed the use of geometrical and analytical techniques and arc lengths to calculate the radial porosity profile of mono-sized spheres in cylindrical packed beds. Later, Mueller [53] used a scaling approach method to formulate a modified empirical correlation model for the radial porosity in both the near-wall and far-wall regions in a fixed packed cylindrical bed. Nikola et al. [54] studied the distribution of packing fraction in a very large 3D heap of monodisperse spherical particles and revealed that the packing fraction of a single-particle sandpile can be divided into four distinct packing density regions. The authors used the Visscher-Bolsterli (VB) algorithm, which provides a realistic framework for rapid computation and allows investigating very large assemblies of particles.

Many researchers [13, 31, 55] also studied factors that affect bed porosity or packing density. Zhou et al. [31] studied the relationship between packing fraction and ellipsoid particle sphericity varied with the packing method and particle shape by the use of DEM. They also studied the effects of particle properties, such as sliding and rolling friction and Young's modulus on the packing fraction. In general, increasing these properties can decrease packing fraction. Tangri et al. [56] investigated the packing behavior of cylindrical particles via both DEM simulations and complementary experiments. They found that packing density increases with the drop height, fill height, container size and coefficient of restitution and decreases with coefficient of friction, surface roughness and Young's modulus. The impact of particle properties on the packing and the packing structure is a fundamental problem relevant to a large number of industries. For example, porosity is a significant property in gas-solid processes encountered in chemical reaction engineering [57, 58]. In blast furnace ironmaking, stock properties and the structure of the lumpy zone have great effects on the voidage in the burden layers, which determines gas distribution and affects the rate of the chemical reactions between particles and the gas. Furthermore the permeability of the burden influences the smoothness

of operation and stability since changes in the pressure drop may cause disturbances, such as gas flow channeling, as well as hangings and slips of the burden.

In studies of heaps of granular material, it is instructive to investigate the formation of a heap when particles are fed onto a horizontal plane and stacked into a conical structure. The angle formed by the surface of the accumulated heap and the horizontal plane is the angle of repose, which is related to the particle density, particle size, the surface area, the shape of the particles and the friction coefficient of the material, etc. The exact definition of the angle of repose varies in the literature, depending on the application it is used for, and how it is measured. According to the different methods, the angle of repose can be divided into four main types of heap formation [59]: static angle of repose by the hollow cylinder method (Figure 12a), pouring angle of repose by the fixed funnel method (Figure 12b), drained angle of repose by the internal flow funnel method (Figure 12c) and the dynamic angle of repose by rotating drum method (Figure 12d). The angle of repose is a fundamental property of a heap, which usually reflects the liquidity potential of it. It has been found that the angle of repose increases with the increase of sphericity [9] and sliding and rolling friction coefficients [60] and decreases with increasing particle size and container thickness. It also generally increases with the moisture of the material, particularly for systems with small particles, because of the cohesion forces between the particles. Recently, Dai et al. [61] demonstrated that it is necessary to associate the microscope characteristics to the macroscopic properties of granular heaps, such as the effects of fabric (particle) orientations on the angle of repose. In the DEM simulation research, the angle of repose is usually used for the calibration of DEM parameters (discussed in Section 3.3.2).
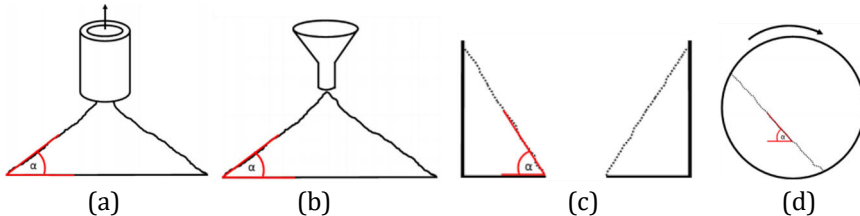

Figure 12. Different types of methods to measure the angle of repose: static angle of repose (a), pouring angle of repose(b), drained angle of repose (c), and dynamic angle of repose (d) [59].

3.2 Modelling of burden and gas flow

Burden charging from the top charging system in the blast furnace plays an important role for the operation of the process. Different charging methods and charging programs lead to different burden distribution in the blast furnace throat. As noted earlier, there is a strong connection between the overall furnace behavior and the burden bed properties. The burden bed at the top of the BF consists of alternate ore and coke layers. Small-scale experiments as well as results from excavated quenched industrial blast furnaces [62] have demonstrated that this layered structure tends to persist during the descent in the BF throat and shaft.

The burden distribution after charging and during descent has been studied by many investigators over the years. Some researchers used burden profile [63, 64], ore-to-coke ratio [65, 66] or porosity distribution [67, 68] to characterize the burden distribution at the upper part of the BF. Size or mass segregation, coke layer collapse, and formation of mixed layers are also important issues that have been studied. To understand the inner state of the blast furnace. The burden distribution can be indirectly estimated by observing the bed surface by radar or mechanical profile meters [69, 70], based on which layer thicknesses can be estimated, but the internal structure can only be accessed by extremely time consuming sampling after filling of the BF before a blow-in; there are no reliable methods by which the internal bed structure can be measured in an operating blast furnace. The only internal measurement seems to be the tracking of ore layers by sensors based on magnetism, discussed in [71], but the method has only been applied at the upper shaft wall and can therefore provide a view of the local properties and not the layer distribution over the whole radius.

To save the effort and time of experimental measurements, a large number of mathematical models of the burden distribution have been proposed. These include data-driven methods [72, 73] and first principle models [74, 75]. Traditionally, these models are empirical or semi-empirical models, correlating results from experiments, or first principle models treating the solid phase as a continuum. However, the assumption that the solid phase is a pseudo liquid, which is not particularly useful for proving understanding of the complex interaction between different burden materials, such as percolation and mixing, so it is almost impossible to predict, e.g., the voidage distribution by traditional models. Along with the development of software and computing power, numerical simulation methods have become a choice for more researchers, such as continuum model [76] and DEM simulation [66, 77]. The combination of these two methods can simulate the gas-solid flow and help understand the inner state of the blast furnace. Some researchers [78, 79] have concluded the burden distribution models, which gave us a deeper understanding and shed more light on the development of the blast furnace ironmaking.

3.2.1 Burden distribution

(1) Burden segregation
For modelling of the upper part of the blast furnace, many researchers have paid attention to the burden charging and discharging and burden distribution in the blast furnace throat. Size segregation occurs in the top bunker and hoppers of the bell-less charging system and in the blast furnace throat where the burden is distributed from the rotating chute. A full-model DEM simulation of the burden flow in the upper part of the system is shown in Figure 13, which considers the burden (sinter, pellets or coke) behavior in the surge hopper (top bunker), parallel/series hoppers, rotating chute and blast furnace throat.

The particle size segregation that occurs during burden charging into or discharging from a hopper is an important phenomenon that eventually influences the burden distribution in the chute or at the throat. The segregation data is usually presented by normalized fine (coarse) mass fraction in a segregation index, $SI = x_{\mathrm{i}}/x_f$ [80, 81], where x_{i} is the fine (coarse) mass fraction

in a given sample and x_f is the fine mass fraction initially in the hopper or throat. This method has the advantage of simplicity and intuitiveness and has therefore been used by many researchers. The relative particle size (RPS) [23, 82] based on mass is another parameter, which is more commonly used to describe the discharging behavior. In general, the larger particles roll outwards near the side wall during flowing on the heap and therefore tend to be discharged towards the end. Fine material remains on the point of impact. Therefore, when reclaiming material from stock, it is important to avoid high amounts of fines being sent to the furnace without screening. In addition, particles move towards the center of the blast furnace as the number of chute rotations increases.

Some researchers investigated the segregation of granular materials during discharging from a hopper using spherical particles of three sizes and the results were also verified by small scale experimental results. Some influencing factors, such as particle diameter ratio, density ratio, fines mass fraction, hopper wall angle, hopper cross-sectional shape, particle friction coefficients and the initial fill conditions were considered. However, most of particles in actual production are irregularly non-spherical particles. Yu and Saxén [83] studied the size segregation of four shapes of coke in the hopper. They found that particle shapes had quite small effect on the simulated size segregation. Later, researchers have carried out large scale simulation of the system. For example, Xu et al. [24] established a full (1:1) scale DEM model of an actual charging system with the particle number exceeding 500,000 to quantitatively evaluate particle size segregation during the charging process. The authors confirmed that large-sized particles dominate the outer granular flow, and form the bottom layer of the packed bed. By contrast, the small-sized particles mainly occupy the inner flow, and they accumulate and cause serious size segregation in the upper layers. Mio et al. [84] used a large 1:3 pilot model of the furnace top for investigating the radial burden distribution and used the experimental findings to validate a DEM model.
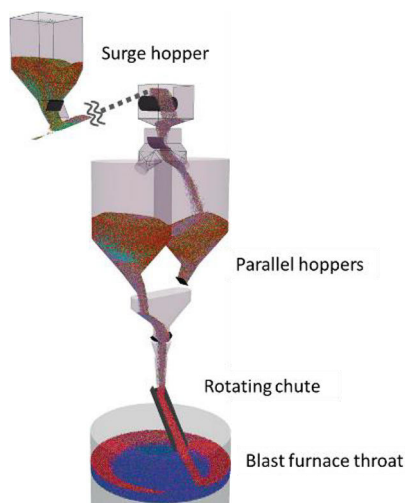

Figure 13. Snapshots of the full simulation model of the particle flow for a bell-less type charging process of a blast furnace.

(2) Burden descent

The radial ore-to-coke mass ratio is an important factor, which can be used to quantitatively reflect the burden distribution. Many researchers have investigated it by different methods, such as probe measurement [85, 86], theoretical analysis [87] and numerical simulation [88, 89]. The ore-to-coke ratio is influenced by the ore batch size, burden size, mixed layer and coke collapse, etc. In addition, the burden bed continuously descends and the burden distribution may change due to the effect of shaft angle that increases the shaft cross-sectional area [88] and by the burden "consumption" due to softening, melting and gasification. The percolation behavior of small size ores in the coke layer during burden descent in the blast furnace [90] also influences the ore-to-coke ratio.

According to measurement results in actual blast furnaces, the burden descent rate near the furnace wall may be up to 50% higher than in the center of the furnace [91]. Cold blast furnace model experiments [92] have also demonstrated that the burden particles near the burden surface at the furnace top do not descend uniformly at different radial coordinates. Mathematical modelling has been the common method for studying the effect of uniform and non-uniform burden descent [93, 94]. Zhou et al. [73] and Chen et al. [95] summarized the development of burden descent models, from applying equal descent rate along the radial direction (Figure 14a) [96] to a linear rate gradient (Figure 14b) [97] to a separate analysis of individual regions (Figure 14c) [92] and ultimately to introducing a relative burden descent rate coefficient K_b to consider non-uniform descent (Figure 14d) [98]. Along with the development of the descent models, the accuracy of the description of the true descent has improved.
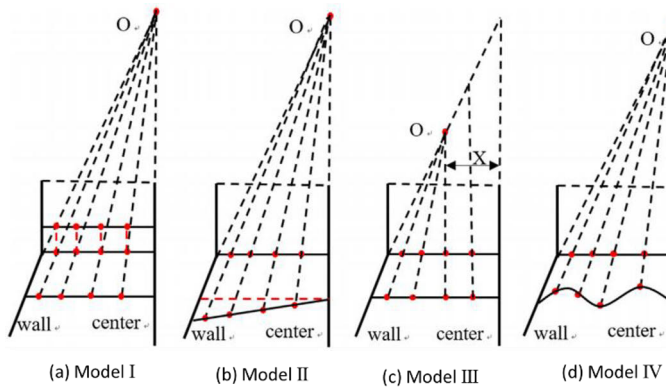

Figure 14. *Burden descent mathematical models [95].*

Using a stock level probe and theoretical analysis, Narita et al. [86] studied the change of layer thickness for different descent rates, $V_c > V_w$ and $V_c < V_w$, where V_c and V_w represent the central and peripheral descent rate, respectively. They found that the layer thicknesses of the charged ore and coke varied with the burden descent rate. And the results obtained from the theoretical analysis are in good agreement with the operational results of the blast furnace. The influence of different descent rates on the radial ore-to-coke ratio was also

studied by Dong et al. [94], who found that the ore-to-coke ratio decreases in regions with slow descent and increases in regions of high descent. They attributed the reason to the angle of repose for ore is smaller than that of coke, leading to further spreading of ore from the impact point. More ore will be charged into the locations where the descent rate is larger.

Many cold physical experiments have been undertaken to prove the validity of mathematical models. However, simplified or continuum models cannot be applied to study complex behavior such as coke collapse, particle segregation and permeation, which affect the final burden distribution. DEM simulation [99] makes it possible to study such complex particulate flow problems. This method has today already been widely used to study local or global particulate and multiphase flows in the BF under different conditions. The development and application of simulation methods in the ironmaking BF have been summarized by many researchers [2, 3, 100]. Zhou et al. [78] used DEM with a 2D slot model to investigate the solid flow in a model blast furnace and validated the results by comparing them with solid flow patterns in experiments conducted under comparable conditions. The simulated movement of the solids from initial to steady state in the BF is shown in Figure 15, where particles charged at different moments have been colored differently. The steady state here means that the flow state when the change in the stagnant zone is not macroscopically observed and the burden layer structure becomes stable. The burden descent in the real BF shaft is mainly due to coke combustion and gasification, as well as ore smelting. In the simulation, particles are commonly discharged from the pre-set raceway regions (cf. white rectangles in Figure 15a) while ore particles can be deleted at a predefined cohesive zone to simulate the downward motion of the bed. Narita et al. [86] studied the influence of variation of the descent velocity on the behavior of burden bed in the blast furnace by comparing the results of descending behaviors with 3D DEM and a semicircular cold model. They found that the difference in descending rate between the central and the peripheral parts results in variation of the distribution of the ore-to-coke ratio.
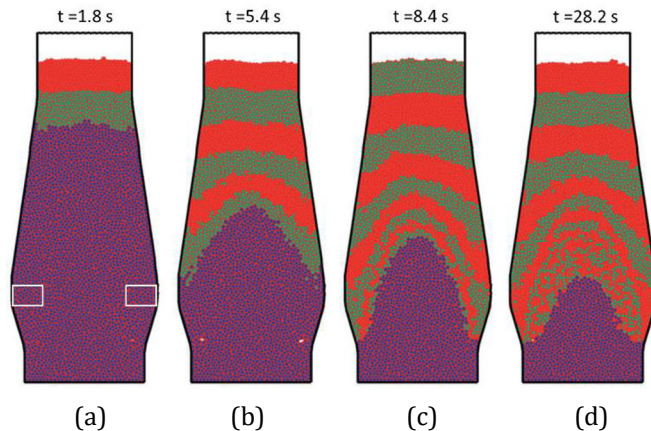

Figure 15. *Snapshots of solid patterns from initial (a) to steady state(d) in a 2D slot model [78].*

To study the actual burden descending behavior, Mio et al. [89] enlarged the simulation to the actual geometry with a width of 10 m and depth of 4 m, under conditions of actual operation. The melting behavior of iron ore and combustion of coke in the actual blast furnace were modeled by shrinking particles. Figure 16 shows the field of mean descent velocity: the velocity increases with increasing distance from the center, and the velocity near wall is much larger than in the center.
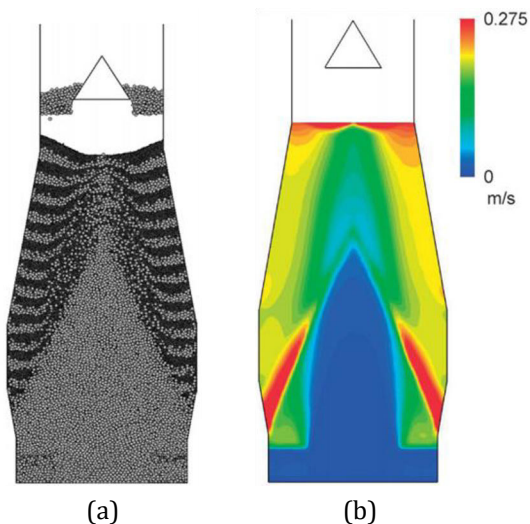

(a)   (b)

Figure 16. *Snapshots of solid pattern (a) and fields of mean velocity of solid (b) in a simulated blast furnace [89].*

(3) Mixed layer and coke collapse

As mentioned above, the size segregation in the burden bed will cause different burden bed structure, and thus the porosity distribution in the alternating layers is strongly heterogeneous in both the axial and radial directions. Mixed layers, which mainly occur at the interfaces of coke and ore (cf. right panel in Figure 17), have been found to show lower voidage than the individual layers and thus higher pressure drop, preventing gas flow and delaying the heating of the burden.
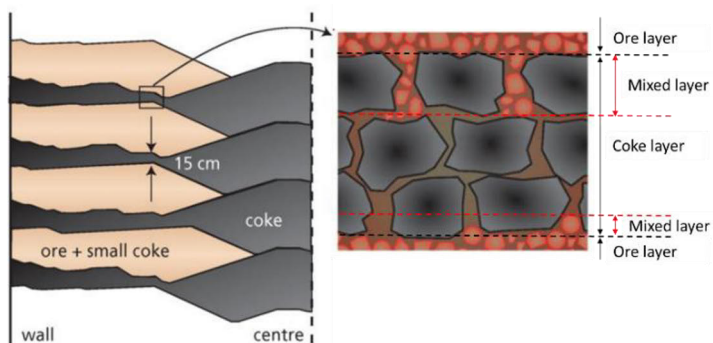

Figure 17. *Formation of the mixed layers: ore burden penetration in coke layer.*

Since the overall performance of the BF is closely connected with local burden properties through their gas permeability, the Ergun equation [101]

$$\frac{\Delta P}{H} = 150 \times \frac{\eta v (1-\varepsilon)^2}{(d_e \varphi)^2 \varepsilon^3} v + \frac{1.75(1-\varepsilon)}{d_e \varphi \varepsilon^3} \rho v^2 \qquad (2)$$

has often been applied to predict the global pressure drop in the furnace using a constant value of the voidage in layers. In the equation, Δp is the pressure drop, H is the height of the burden bed, η is the dynamic viscosity of gas, v is the superficial velocity of the gas, ε is the burden void fraction, d_e is the equivalent sphere diameter, φ is the sphericity and ρ is the density of the gas.

From this equation, it can be seen that even a small decrease in the voidage along the vertical or radial direction of the bed will significantly influence the permeability of the whole bed, and thus also the gas flow. Figure 18 shows the effect of porosity on pressure drop gradient of BF when d_e = 30 mm, φ = 0.72 and ρ = 1.29 kg·m^{-3}. Obviously, the permeability increases with the increase of the porosity. When the porosity drops below 0.3, the permeability of the burden bed deteriorates sharply, which will have large impact on the distribution and temperature of the gas flow. In general, the gas permeability of a coke layer is considerably higher than that of an ore layer, and mixed layers of coke and ore have been found to show lower voidage than for two individual layers, preventing gas flow and delaying heating of charged materials [102].
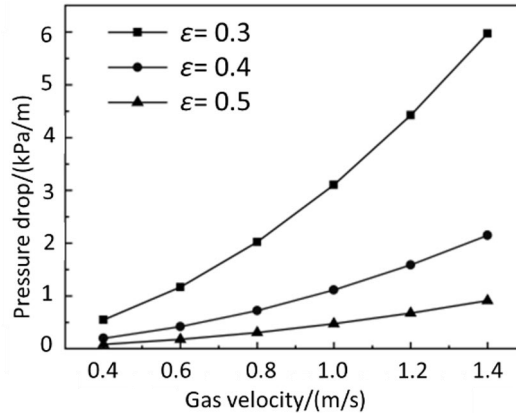

Figure 18. *Effect of porosity on pressure drop gradient of BF.*

Factors influencing the inter-particle percolation of small particles (pellets) into a layer of larger particles (coke) during burden descent have been investigated in earlier work. Yu and Saxén [103] demonstrated that the coke shape, pellets diameter, static friction and inter-particle rolling friction and restitution had marked effects on the percolation. The dynamic evolution of the mixed layer during the charging process was also analyzed based on a 1:10 charging model [102]. Non-spherical particles [104] and particles under wet/dry condition have also been considered [105]. However, these studies were mostly conducted under simplified conditions, for example, ignoring the influence of the forces from the gas flow and physical or chemical reactions between different phases. There is also little research on the formation of mixed layers in the BF

and its effect on the whole BF performance. E [98] used a combined computational fluid dynamics and discrete element method to investigate the porosity distribution and pressure drop of the mixed layer, by considering the lumpy and cohesive zone. This can give more realistic view of the BF state than that by modeling conducted under more simplified conditions. The results showed that the gas flow can significantly affect the mixed-layer properties. The occurrence of mixed layers increases the complexity of the burden structure and also makes it more difficult to describe the true conditions mathematically. Understanding the structural features of the mixed layer is therefore important in research on the distribution of the gas flow in the lumpy zone.

Besides mixed layers, "coke collapse" is also a common phenomenon for the layered burden bed. Since sinter or pellets are about four times heavier than coke, they may upon charging push the coarse coke particles on the top of the coke layer towards the center, resulting in what is also called "coke push" (cf. Figure 19c). The most immediate effect of this phenomenon is that it results in a higher coke fraction near the center of the furnace than expected. Describing this effect is a complication as the burden profile may vary strongly depending on the charging program and burden size, and it is difficult to quantify the effect. Some researchers utilized the stability theory of slopes to determine if a layer would be stable upon charging of a pellets layer [106, 107]. Mitra and Saxén [102, 107, 108] observed the "coke push" in a small-scale experiments and further investigated and quantitatively described the "push" effect by DEM.

(a)

(b)   (c)
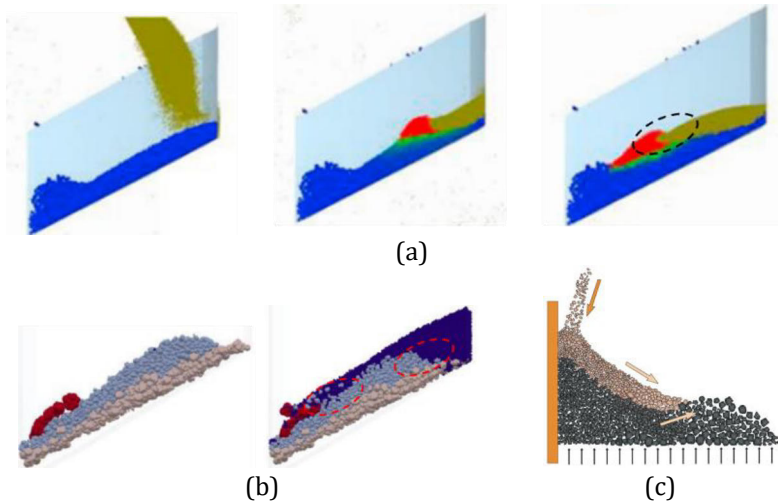
Figure 19. Pellets pushing coke layer to the center (a). Red denotes coke particles with high velocity, and blue denotes stationary particles [108]. Before and after charging ore to coke layer [102] (b). Coke push effect [17] (c).

From the Figures 19a and 19b, there is a significant difference between the coke layer shape before and after charging. It is evident that the pellets dumps have moved the coke from the wall towards the center of the furnace. Zhou et al. [77] divided the burden bed into different zones along the radial direction of the throat to estimate the change of the coke quantity in the different zones. After a sensitivity analysis, the investigators found that reverse charging (i.e., with

decreasing chute angles) decreases the extent of coke collapse, and that central-coke charging of as little as 5 wt % of the coke also significantly reduces the coke collapse.

3.2.2 Gas flow distribution

The blast furnace is a large-scale reactor with solids, liquids and gas, with comprehensive physical and chemical reactions and heat transfer. Gases inside the blast furnace arise partly from the externally supplied hot blast and partly from the internal reactions of combustion, reduction and coke gasification [109]. Figure 20 shows a gas-solid contact and reaction diagram of a simplified blast furnace. The burden distribution determines the gas distribution through the permeability (porosity) of the individual layers and thus influences the particles in contact with gas flow for the heat transfer and gas-solid chemical reactions. Different porosity distribution due to burden distribution will cause different gas distribution and thus also different local gas velocity (cf. Figure 21), with stronger gas flow in regions with a lower ore-to-coke ratio [76].
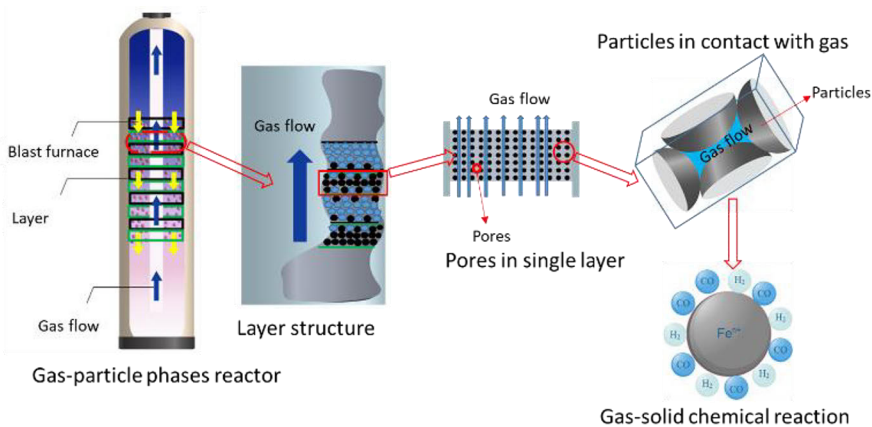

Figure 20. *Gas-solid contact and reaction diagram in blast furnace.*

Mathematical modeling, often coupled with physical modeling, has become the most effective and reliable method to study the gas flow distribution and the internal variables in the blast furnace [110]. The discrete element method has mainly been used to analyze the motion of solid particles and the influence of the interaction between particles in the furnace on the burden movement, while continuum methods have been used to describe gas flow and the flow of solids was treated as a pseudo fluid, with heat and mass transfer and chemical reactions between different phases in the furnace. Therefore, a combination of the two methods has attracted recent attention. By this, the microscopic behavior of particles in the blast furnace can be captured, with a behavior showing closer resemblance with the actual motion state of charge and gas. Therefore, the CFD-DEM simulations have a better potential to describe the true behavior of the phases in the blast furnace process.
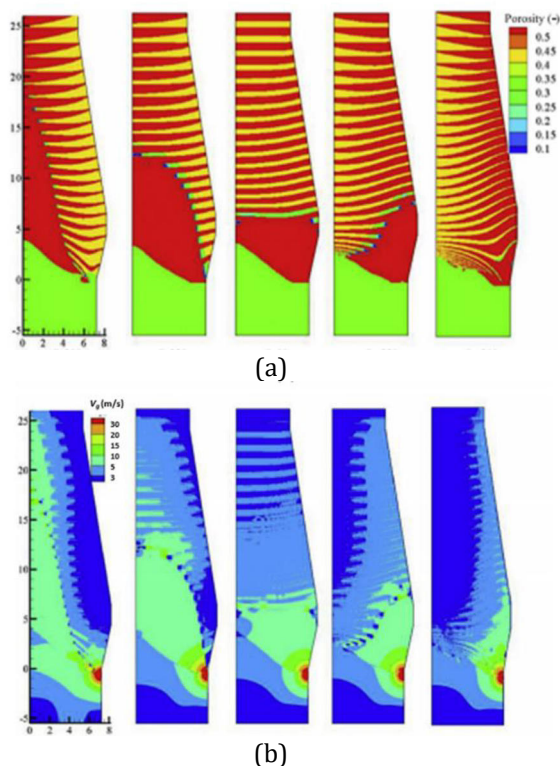
(a)

(b)

Figure 21. *Predicted spatial distributions of porosity (a) and gas flow (b) within the BF operated with different top burden distributions [76].*

A majority of the CFD-DEM models reported for the blast furnace have been based on 2D slot models to reduce the computational demand. Hou et al. [110] successfully developed a 2D CFD-DEM model to simulate the multiphase flow and thermochemical behavior. The simulated results were compared with the temperature measured by a vertical probe located in the center of the LKAB experimental furnace and the predicted results were observed to qualitatively agree with that of the measured ones. 2D models have been more widely used for research on the gas flow in the upper shaft and throat of the BF, while 3D sector or full models have usually been used when considering the coke combustion in the raceways and the coke motion below the cohesive zone, since such models can supply more comprehensive multi-flow information than 2D models. Sector models are established based on the fact that the flows along the circumference can largely be regarded as symmetrical. Compared to full models, sector models have obvious advantages in reducing the computation time. It has been demonstrated that the flow patterns predicted by sector models are very close to those of full models [111]. Bambauer et al. [112] investigated the gas and solid flow as well as the liquid accumulation with a full 3D model of a (down-scaled) BF and the results were compared with 2D slot BF simulations performed by Zhou et al. [113]. The results showed that the proposed simulation approach is capable to reproduce the main phenomena in a down-scaled isothermal BF.

3.3 DEM equations and parameters

3.3.1 Discrete element method

The Discrete Element Method is one of the most popular ways for simulating granular systems. It was firstly proposed by Cundall and Strack [99] in 1979. In spite of the fact that the computational requirements still limit the applicability of this technique, DEM has today become a viable tool for analyzing and describing the behaviors of granular matter mathematically. The force acting on each particle is modeled and calculated at each discrete time step. The position of the particle is updated by Newton's law of motion in this process. The interaction forces of two particles in contact are shown in Figure 22.
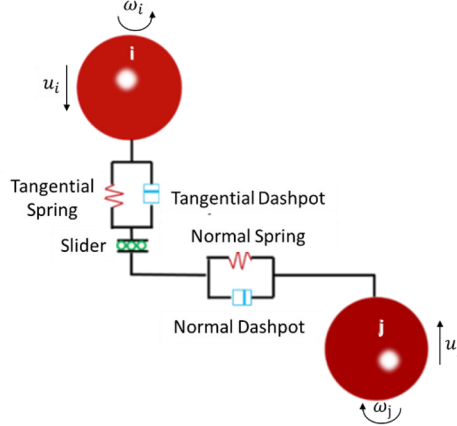

Figure 22. Depiction of interaction forces between two particles (i and j) in DEM.

DEM recognizes two motion states of particles: translational and rotational. In this work, the open source software LIGGGHTS [114] with the Hertz-Mindlin contact model was used. This DEM tool is an extension of the basic molecular dynamics code LAMMPS, which is commonly used to describe granular matter and granular heat transfer. The governing equations for the motion of particle i with mass m_i and moment of inertia $\boldsymbol{I}_i$ in contact with N other particles j can be written as

$$m_i \frac{d\boldsymbol{u_i}}{dt} = \sum_{j=1}^{N}\left[\left(\boldsymbol{K}_{\mathrm{n}}\delta_{\mathrm{n},ij} - \boldsymbol{\gamma}_{\mathrm{n}}\boldsymbol{v}_{\mathrm{n},ij}\right) + \left(\boldsymbol{K}_{\mathrm{t}}\delta_{\mathrm{t},ij} - \boldsymbol{\gamma}_{\mathrm{t}}\boldsymbol{v}_{\mathrm{t},ij}\right)\right] + m_i\boldsymbol{g} \qquad (3)$$

$$\boldsymbol{I}_i \frac{\mathrm{d}\boldsymbol{\omega_i}}{\mathrm{dt}} = \sum_{j=1}^{N}(\boldsymbol{M}_{\mathrm{r}}^{\mathrm{k}} + \boldsymbol{M}_{\mathrm{r}}^{\mathrm{d}}) \qquad (4)$$

where $\boldsymbol{g}$, $\boldsymbol{u}_i$ and $\boldsymbol{\omega}_i$ are respectively the gravity acceleration, translational and angular velocities of the particle i. δ_{n} expresses the overlap distance of two particles, $\boldsymbol{v}_{\mathrm{n}}$ and $\boldsymbol{v}_{\mathrm{t}}$ represent the normal and tangential components of the relative speed of the two particles. $\boldsymbol{M}_{\mathrm{r}}^{\mathrm{k}}$ and $\boldsymbol{M}_{\mathrm{r}}^{\mathrm{d}}$ are, respectively, the spring torque and viscous damping torque. For the alternative elastic-plastic spring-dashpot (EPSD2) model [115], which was used in this study, the viscous damping torque $\boldsymbol{M}_{\mathrm{r}}^{\mathrm{d}}$ was disabled.

The elastic contact theory of Hertz [116] was adopted in the DEM simulations to calculate the inter-particle elastic contact force in the normal direction with the normal elastic constant, K_n.

$$K_n = \frac{4}{3} \cdot \frac{Y_i Y_j}{Y_j(1-\vartheta_i^2)+Y_i(1-\vartheta_j^2)} \sqrt{\frac{R_i R_j}{R_i+R_j}} \delta_n \tag{5}$$

The tangential elastic contact force was calculated by an improved contact force model [117], Mindlin no-slip solution for tangential particle contact. The tangential elastic constant K_t can be calculated by

$$K_t = \frac{4Y_i Y_j}{Y_j(2-\vartheta_i)(1+\vartheta_i)+Y_i(2-\vartheta_j)(1+\vartheta_j)} \tag{6}$$

γ_n and γ_t are respectively the normal and tangential viscoelastic damping constants [118, 119], which can be calculated by

$$\gamma_n = -2\sqrt{\frac{5}{6}} \frac{ln(e)}{\sqrt{ln^2(e)+\pi^2}} \sqrt{\frac{2Y_i Y_j \sqrt{\frac{R_i R_j}{R_i+R_j}} \delta_n \cdot \frac{m_i m_j}{m_i+m_j}}{Y_j(1-\vartheta_i^2)+Y_i(1-\vartheta_j^2)}} \tag{7}$$

$$\gamma_t = -2\sqrt{\frac{5}{6}} \frac{ln(e)}{\sqrt{ln^2(e)+\pi^2}} \sqrt{\frac{4Y_i Y_j \sqrt{\frac{R_i R_j}{R_i+R_j}} \delta_n \cdot \frac{m_i m_j}{m_i+m_j}}{Y_j(2-\vartheta_i)(1+\vartheta_i)+Y_i(2-\vartheta_j)(1+\vartheta_j)}} \tag{8}$$

where Y, e and v represent properties of particle, i.e., Young's modulus, coefficient of restitution and Poisson's ratio, respectively.

The torque due to the spring M_r^k [120] is calculated as

$$S_r = S_t \cdot R^{*2} \tag{9}$$

$$\Delta M_r^k = -S_r \Delta\theta_r \tag{10}$$

$$M_{r,t+\Delta t}^k = M_{r,t}^k + \Delta M_r^k \tag{11}$$

$$|M_{r,t+\Delta t}^k| \leq M_r^m = \mu_r R^* F_n \tag{12}$$

where S_t is the tangential stiffness and S_r is the rolling stiffness, R^* is the effective radius, and $\Delta\theta_r$ is the incremental relative rotation between the particles. The spring torque is limited by the full mobilization torque, M_r^m that is determined by the effective radius, the normal force, F_n, and the coefficient of rolling friction, μ_r.

The friction force is expressed with a Coulomb-type friction law. It defines that the tangential force F_t of a particle should be no more than the normal force, F_n, multiplied by the coefficient of static friction, μ_s

$$F_t \leq \mu_s F_n \qquad (13)$$

3.3.2 Calibration of DEM parameters

In the DEM calculation, the geometry, initial conditions and physical parameters have to be preset, where the physical parameters are principal particle properties. The motion of the particles is determined by the force state. Here, the contact force and torque are affected by the properties of the particles. The physical parameters can be divided into two categories. The first category includes contact parameters, mainly coefficients of static, sliding and rolling friction, and coefficient of restitution. The second category includes the particle properties, e.g., particle density and size, Poisson's ratio, Young's modulus and shear modulus.

It is obvious that the appropriateness of the DEM parameter values affects the accuracy of description of the simulated motion of the granular matter. Michele et al. [121] demonstrated that one of the main difficulties for the industrial application of DEM is the calibration of the model parameters. Therefore a clear need exists for robust calibration procedures that are efficient from both experimental and numerical points of view [9]. Many investigations have shown that the simulation results are sensitive to the chosen parameters, including the effects of physical parameters on repose angle and packing density [31, 122]. For instance, Yu and Saxén [103] studied the influence of the DEM parameters on the inter-particle percolation of pellets into coke and found that the pellet diameter, coefficient of static friction and inter-particle rolling friction, and coefficient of restitution had obvious effects on the percolation, whereas the shear modulus was of minor importance.

The most common approach for the measurement or calibration of DEM parameters can also be divided into two categories, i.e., Bulk Calibration Approach and Direct Measuring Approach [123]. The former method measures a specific material bulk property under the same conditions as in an experiment. The DEM parameter values are changed iteratively until the predicted bulk response matches the measured result. As an example, the angle of repose (cf. Figure 23) in simulations and laboratory experiments is applied to determine the coefficient of static or rolling friction between particles and between particle and wall [59, 124]. The problem of this method is that the bulk property is usually not determined by a single parameter, but by a combination of multiple parameters. In the second method the property values on particle or contact level are directly measured. This approach is only accurate if the shape and size of the particles are modelled accurately and if the contact model is an accurate representation of the physical contact behavior [125]. Obviously, some easily measured parameters (properties) can be determined by this method, while certain contact parameters have to be measured by the former one. For example, the validity of the physical parameters determined in impact load cell tests [126, 127], tribometer tests [128] and drop particle tests [129] should be further verified by comparison of experimental and simulated results. Zhang et al. [130] estimated the cohesion coefficient of mortar particles by comparing the spread diameter and flow time in V-funnel batch experiments and simulation. Wang et

al. [129] presented a method to determine the coefficient of friction of the particle-particle collision of frozen maize in three dimensions. Recently, Agarwal et al. [131] proposed a novel method based on image analysis of static grains to calculate the rolling friction coefficient of particles.
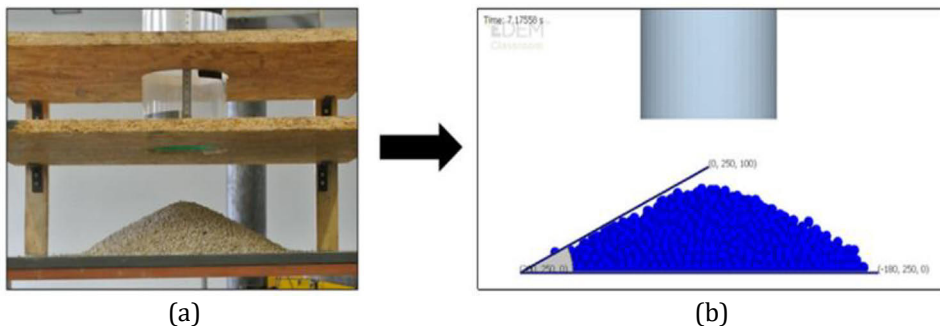

| (a) | (b) |

Figure 23. Angle of repose between laboratory (a) and simulation results (b) [59].

For DEM simulation of particle flow in the blast furnace, the calibration of DEM parameters of burden materials is particularly important. In many DEM studies, the investigators used parameter values taken from the literature without making any attempt to "measure" the parameter values, even though there were some differences between the materials they used and those used in the literature. As a result, the parameters used may be unreasonable, resulting in distortion of the simulation results. Based on this, the calibration of DEM parameters of burden materials is a key and non-ignorable step that is necessary to obtain accurate simulation results. Barrios et al. [125] used a pin-on-disk tribometer to measure the friction coefficient of iron ore pellets. They also used a simple apparatus to measure the rolling angle of particle for the measurement of coefficient of rolling friction and a series of drop particle tests for the coefficient of restitution. Madadi et al. [132] improved this pin-on-disk tribometer method, because they deemed it inaccurate for measuring the friction coefficient using a thin layer of iron ore resin under long and continued contact. Except the contact parameters between the same particles, the coefficient of rolling and static friction between different types of particles as well as between particles and wall were also studied [133]. Some researchers have summarized the application of different measurement methods for different DEM parameters [123] and the measured values of the main blast furnace burden materials [95].

Particle shape is also an important parameter for the DEM simulation. For large scale particle systems, researchers often use spherical particles with adapted coefficient of rolling friction to characterize the actual particle shape. This simplified method can reduce the computational overhead, but the real shape of the burden material is ignored. Wensrich and Katterfeld [134] considered using friction coefficients to consider the influence of shape. The results showed that in simple cases, using the coefficient of rolling friction as a "tunable parameter", spherical particles can implicitly consider the effect of shape. However, for certain phenomena the effect of particle shape may be minor. Yu and Saxén [83] used coke particles with four kinds of shapes to simulate the segregation behavior of particles during charging and discharging of a hopper.

After comparing the simulated results with the experimental ones, it was found that the particle shapes had little effect on the simulated size segregation and the authors concluded that spherical particles can be used to estimate the segregation of coke particles during hopper charging and discharging.

4 Main work of the thesis

The structure and behavior of particle heaps using DEM simulation were mainly studied in this thesis. The results were calibrated by a series of different experiments in small scale. After this, the research method and DEM model of the particle heap were applied to blast furnace burden simulation. Further, the DEM parameters of main blast furnace burden materials were measured to ensure the accuracy of the blast furnace simulation results. A flowchart of the research contents of this thesis is shown in Figure 24: the numbered papers refer to the publications in the Appendix.
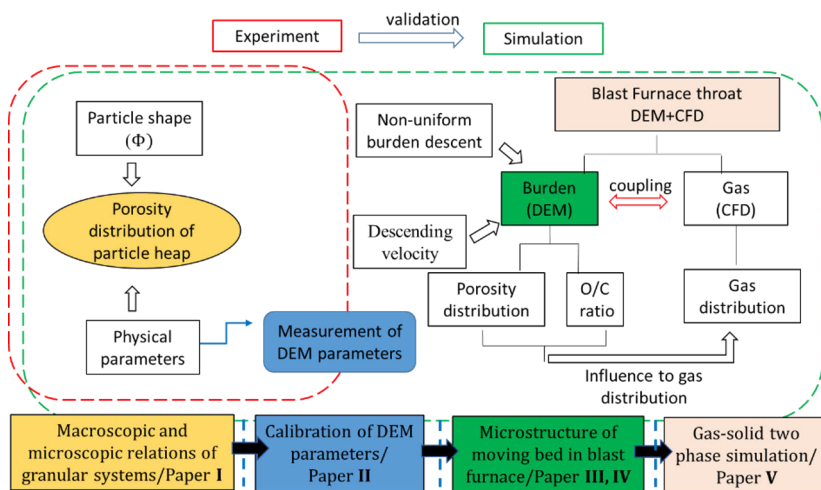

Figure 24. Flowchart of the research in this thesis.

Firstly, the DEM model based on a particle heap formed by natural accumulation was established. The effects of particle properties on repose angle and porosity distribution of iron ore heaps were studied by experimental and numerical methods. Spherical, cylindrical and conical iron ore particles with the same (bottom) diameter and height, but with different sphericity, were used to describe different particle shapes. This part of the study serves to clarify the influence of using spheres in DEM models to describe actual particles in industrial applications on the internal structure of the particle heap, e.g., porosity and angle of repose.

Secondly, since the DEM parameters play an important role for the accuracy of the simulations, some parameters of the commonly used burden materials were determined by testers or experiments with homemade devices. On the basis of the results obtained in the small-scale experiments, the DEM models were evaluated under different parameter settings (e.g., for static and rolling frictions, as well as restitution coefficients) to determine the model parameter combinations that provided the best agreement between simulated and experimental results.

The layered structure applied in the blast furnace, with alternating layers of coke and ore, has implication for the properties of the burden bed, including porosity distribution and radial ore-to-coke ratio in the throat, both after the

burden charging and during descent. In order to shed more light on the overall performance of the upper part of the blast furnace with a bell-less burden charging system, two-dimensional (2D) slot throat model and three-dimensional (3D) sector throat model were established to study the properties of burden structure. A laboratory bell-less charging system with a scale of 1:10 compared to an industrial BF was designed and used for some small scale experiments of burden charging and descending. Furthermore, the intermittent charging and continuous descent of burden, and the simultaneous ascent of gas through the particle bed were simulated with a combined CFD-DEM model. The model captures the complex interaction between the solid and gas flows, which affects the radial temperature distribution due to heat transfer and gas redistribution.

4.1 Experiments and DEM modelling of the heap (Paper I)

4.1.1 Preparation of non-spherical particles

Heaps of iron ore particles were formed by small scale experiments and DEM simulation. Based on this, the effects of particle properties on repose angle and porosity distribution of the heaps were studied by DEM. Spherical, cylindrical and conical iron ore particles with the same bottom diameter and height, but with different sphericity (1.0, 0.86, and 0.67, respectively) were prepared in the laboratory to represent different particle shapes. The preparation of non-spherical particles includes the materials preparation for experiments and the establishment of the non-spherical particle models for DEM simulations.

A. Material preparation in the laboratory

Pellets were used to represent spherical iron ore particles, and were obtained from a steel plant in China and the selected particle size was 13-15 mm after sieving. In order to avoid the effects of particle shape, almost spherical pellets were selected for the physical experiments. The cylindrical and conical iron ore particles, which have the same bottom diameter (14 mm) and height (10 mm), were produced in the laboratory imitating the preparation conditions of pellets. The green particles were created in cylindrical or conical molds and were then subjected to high temperature (1250 °C). Simple drop tests were carried out and only slight cracks on the particle surface were found after dropping the particles more than 50 times, which demonstrated that the prepared particles had enough strength for the experiments in this research. The number of spherical and cylindrical particles is 5000 and the number of conical particles is 10000.

B. Non-spherical particle model

Single sphere was used to represent pellets in the simulations. For non-spherical particles, multi-sphere clusters were applied to mimic the real particle shapes, which are shown in Figure 25. In order to ensure the consistency of the experiments and simulations, the particle sizes used in the simulations were the same as those of the experiments. The number of glued spheres applied were chosen to be sufficient to represent the real shape still keeping the number reasonable: increasing the number of small spheres will increase the accuracy of the particle model, but at the same time it increases the calculation time.
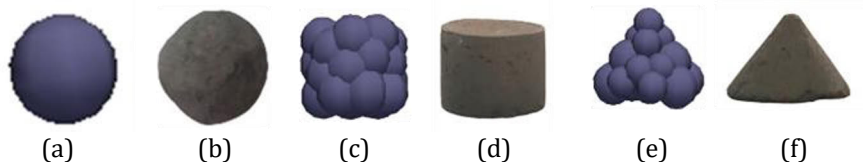
(a) (b) (c) (d) (e) (f)

Figure 25. Comparison of spherical and non-spherical particle shapes in the simulations (a), (c) and (e) and in the experiments (b), (d) and (f).

4.1.2 Heap formation and processing of results

The formation methods of the heap in the experiments and simulations were the same, i.e., the fixed funnel method. Therefore, the angle studied in this research was the pouring angle of repose. The experimental apparatus and geometry model applied in the simulations are shown in Figure 26. The process is simple: particles were gathered in a hopper and then a baffle at the exit of the hopper was removed and the particles were discharged on the table to form a heap.
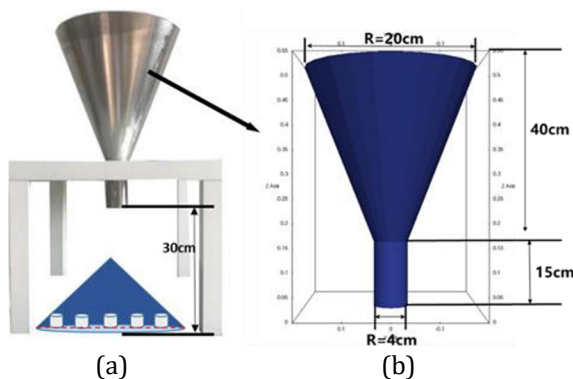

(a)   (b)

Figure 26. Experimental apparatus, including emptying device and BPD measuring device (a). Dimensions of the hopper used in simulations, which are the same as that used in experiments (b).

As for determining the porosity, different methods were applied in the experiments and simulations. In simulation, five virtual boxes with the dimensions of 5 cm × 5 cm × 7 cm for spheres or cylinders and 5 cm × 2.5 cm × 7 cm for cones on the central line of the bottom of the heaps were used to calculate bottom porosity distribution (BPD), which are shown in Figure 26a. However, in experiment, sample beakers were buried along a bottom line of the heap in advance to measure the porosity distribution. The volumes of the beaker are respectively 25 mL (spheres and cylinders) and 15 mL (cones). Beakers fully filled with particles were finally gently removed from the heap to estimate the porosity distribution. The porosity was measured by a drainage method and can be calculated by

$$P = \frac{V_0}{V} \times 100\% \tag{14}$$

where V_0 is the volume (mL) of pores obtained by measuring the volume of water with particles in beakers, and V is the volume of the empty beaker (mL). For the simulation, the porosity was calculated by

$$P = 1 - \Sigma \frac{n_i V_i}{V_{\text{box}}} \tag{15}$$

where n_i expresses the number of particles of type i and V_i is the volume of the particle, while V_{box} is the volume of the virtual box.

Photographs of the heap shapes from two different directions were taken by a fixed camera at the level of the table, and the photos were processed to determine the angle of repose by extracting the contour of the heap.

4.1.3 Angle of repose of the heap

Figure 27 shows the effects of the coefficient of static friction (μ_s) and the coefficient of rolling friction (μ_r) on angle of repose of heaps formed by particles of different shapes. It can be seen that when the μ_r is larger than 0.2, the influence of μ_s on spherical particle heaps is greater than for non-spherical particles. When μ_s changes from 0.01 to 0.4, the angle of repose of heaps of spherical and non-spherical particles increased by about 20° and 15°, respectively. The effect of μ_r on the angle of repose is relatively small compared to the effect of μ_s. As expected, spherical particles give rise to the lowest angle of repose compared with the other two shapes, because non-spherical particles are more easily to lock on the slope due to the existence of edges, making the heap steeper. However, the repose angles of heaps of cylinders and cones are very close to each other since they have the same size and particle properties. Furthermore, when μ_s is small, the effect of μ_r on angle of repose becomes stronger if the particle shape deviates from spherical. From Figure 27, it can be observed that when $\mu_s > 0.2$ and the μ_r is large, the growth rate of the angle of repose slows down. Especially for high rolling friction (Figure 27c, $\mu_r = 0.6$) the repose angles for heaps of spheres and cones remain stable.
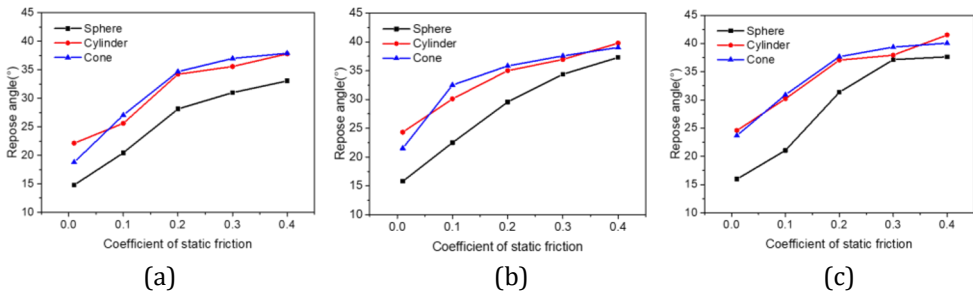

Figure 27. Relationship of angle of repose and particle shape for different static and rolling friction: $\mu_r = 0.2$ (a), $\mu_r = 0.4$ (b) and $\mu_r = 0.6$ (c).

Compared with the particle shape and coefficient of rolling friction, the coefficient of static friction has the largest effect on the shape of the heap (angle of repose). When comparing the repose angles of the heaps from experiments and simulations with different coefficients of friction for the three kinds of iron

ore particles, an appropriate combination of μ_r and μ_s (cf. Table 2) can be determined and used for future research (e.g., to determine the porosity).

Table 2 *Coefficients of friction (μ_r and μ_s) of heaps of spheres (pellets), cylinders and cones.*

Particles	Coefficient of static friction	Coefficient of rolling friction
Sphere(pellets)	0.4	0.2
Cylinder	0.3	0.2
Cone	0.3	0.4

4.1.4 Radial bottom porosity distribution of the heap

Figure 28 shows a comparison of the bottom porosity distribution (BPD) of the experiments and simulations, where the coefficients of friction were those reported in Table 2. To maintain consistency between the experiments and simulations, the porosity in Figure 28 was obtained for a simulated container whose size is the same as the beakers used in experiments. The results are seen to show good consistency. Overall, the porosity increases from the center to the edge of the heap and displays a V-shape distribution for all three kinds of particles. After the initial formation of a small heap, the heap alternately grows and collapses, and particles slide or roll on the sides from the heap center to form the edges. Therefore, particles in the center of the heap are better configured with surrounding particles and the inner structure is more compact than for the region at the edges.

The effects of the coefficient of static and rolling friction on BPD were also studied. Figure 29 shows 3D graphs of the relationship between porosity and both μ_r and μ_s for the three kinds of heaps. Like for the angle of repose, for all the three particle shapes, μ_s has a greater (and positive) influence on the porosity than μ_r. A large coefficient of friction implies a large friction force, which restricts the relative movement or rearrangement of the particles, and hence a heap of high porosity is generated. When μ_s is small, μ_r shows greater influence on the porosity of heaps of non-spherical particles than on heaps of spherical ones. This results are consistent with the above that of the angle of repose, which reveals the change of angle of repose in the external parts of a heap, in fact, reflects the change of the internal structure (porosity).

In order to clarify the effects of particle shape on porosity of a heap, the results of the experimental study by Zou and Yu [135], the DEM study by Zhou et al. [31] and the present work have been summarized in Figure 30. There is a minimum value of the average porosity of the heap with a change of sphericity φ (found at about $\varphi = 0.85$). The trend reported in the literature is similar to what was found in the present study, but the porosity determined in my work is a somewhat higher (relative difference 13%). A reason may be that the present work focused on the porosity of bulk materials in natural piling, but the references studied compacted porosity in a cylindrical container. It is also worth noting that the cylindrical particle heaps have the smallest porosity among the three shapes of particles, because cylinders with two parallel planes are more easily rearranged in parallel, thus reducing the void between the particles.
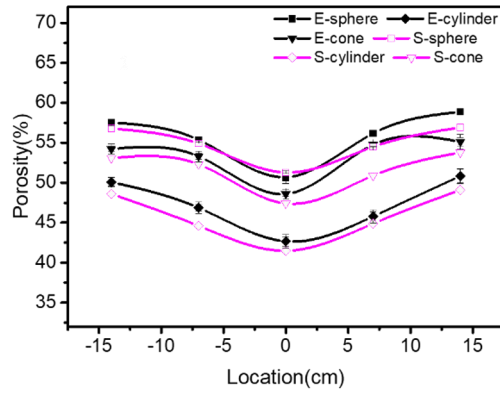
Figure 28. *Comparison of BPD of simulated heaps (with real container) and experimental ones: black curves represent experimental values (E) and red curves represent simulated ones (S) for the three kinds of heaps.*
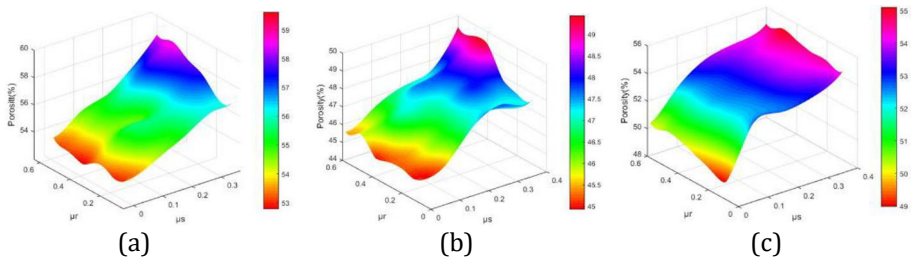

| (a) | (b) | (c) |

Figure 29. *3D graphs of the relationship between porosity and μ_r and μ_s for three kinds of heaps: spheres (a), cylinders (b), and cones (c).*
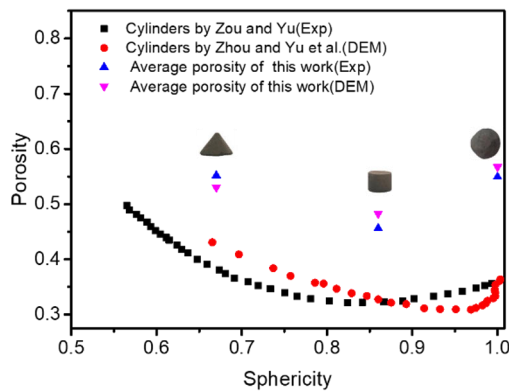
Figure 30. *Relationships of sphericity and average porosity: "average porosity of this work" represents the average value of BPD.*

4.2 Measurement and calibration of DEM parameters (Paper II)

4.2.1 Measurement of DEM parameters of burden particles

In numerical simulations of solid flow in the blast furnace, the DEM is a versatile method, but the accuracy of physical parameters of the method is key for the reliability of the results. Therefore, the parameters describing the interaction

between pellets, sinter and coke, as well as between these three materials and a "wall" material, steel plate, were measured. The experimentally determined parameters include the Young's modulus (Y), Shear modulus (G), Poisson's ratio (v), particle density (ρ), coefficient of restitution (e), as well as coefficients of static and rolling friction.

Figure 31 shows a summary of the measurement methods for mainly DEM parameters of burden particles. In the present research, Y, G and v of pellets were measured by a dynamic elastic modulus tester. Particle density was measured by a true pycnometer based on the principle of the ideal gas law. The measurement values are summarized in Table 3. Coefficients of restitution of pellet-pellet (P-P), pellet-steel plate (P-steel), sinter-sinter (S-S), sinter-steel plate (S-Steel), coke-coke (C-C) and coke-steel plate (C-Steel) were measured by a drop-bounce experiment using a high-speed industrial camera to record the whole process. Coefficients of static and rolling friction for P-P were measured by a simple homemade device combined with a high-speed industrial camera. The coefficients of rolling friction of non-spherical particles (sinter and coke) were obtained by the comparison of the repose angle of bulk materials in experiment and simulation. After these calibration steps, the DEM parameters were validated by the comparison of the free surface of conical heaps formed in simulations and experiments.
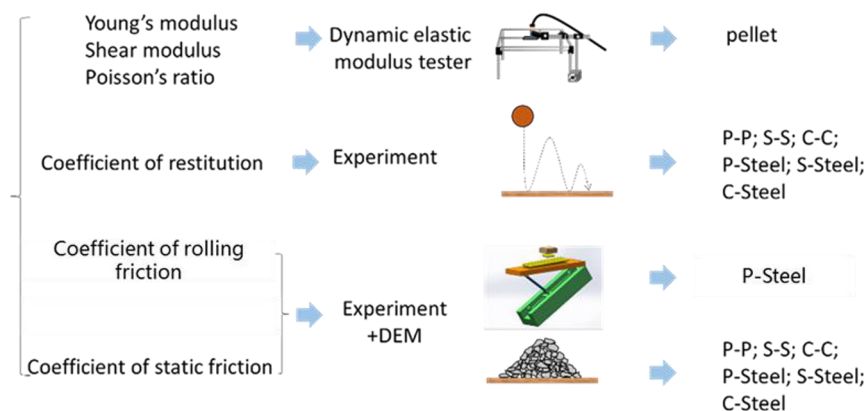

Figure 31. Measurement methods of (mainly) DEM parameters of burden particles. P-P, S-S, C-C, P-Steel, S-Steel and C-Steel represent the coefficients of pellet-pellet, sinter-sinter, coke-coke, pellet-steel plate, sinter-steel plate and coke-steel plate, respectively.

Table 3 Measurement results of properties of pellets.

Properties	Density (kg/m³)	Young's modulus (GPa)	Shear modulus (GPa)	Poisson's ratio
Value	3990	126	50.9	0.24

(1) Coefficient of restitution (COR)

The principle of the measurement of the coefficient of restitution is shown in Figure 32a. The coefficient of restitution defines the ratio of the final velocity (v) to initial velocity (u) between two objects after collision (cf. Equation 16) and is

related to the hardness and shape of the material and the specific features of the collision. It reflects the elastic ability of an object (A) after colliding with another (B) and can be calculated by

$$e = \frac{v_B - v_A}{u_B - u_A} \qquad (16)$$

In the experiments, particles (object A) were dropped onto a fixed table (object B), so v_B and u_B are considered zero. Thus, Equation 16 can be simplified to $e = v_A/u_A$, where u_A and v_A are the instantaneous velocity of particles before and after impacting on the table. It should be noted that velocity here refers to the absolute value, so the direction is not considered.
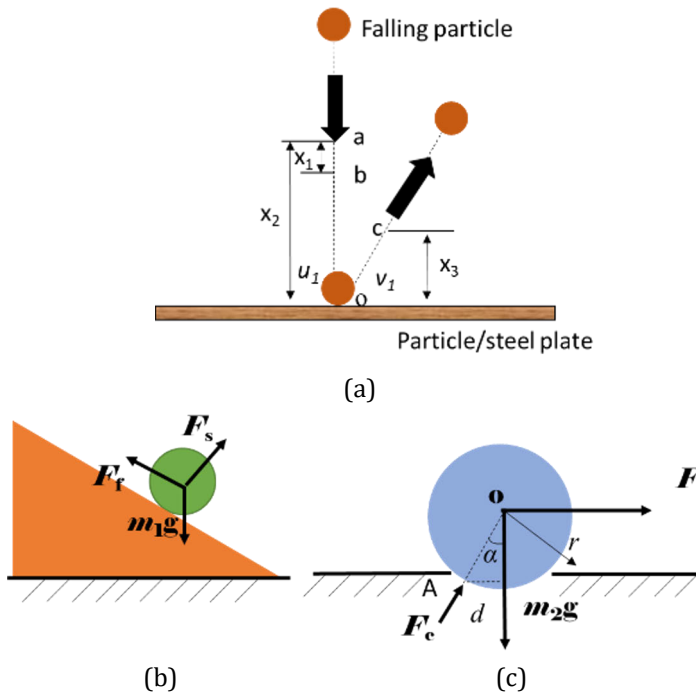

Figure 32. Schematic diagram of the principle of the measurement of coefficient of restitution (a), coefficients of static (b) and rolling friction (c).

Three kinds of "particle plates" were made to measure the coefficient of restitution for particle-particle interaction. The particle plate was composed of a 5 mm thick plank and similar size particles, which were glued on the plank surface. In order to reduce the effects of particle shape, a flat part of each particle was fixed to face upwards on the plate to yield a possibly smooth "table". A high-speed industrial camera was used to record the process and follow the particle trajectory. The relationship between the displacement and time of the movement of particle can be established from the video which had a short time interval per frame (1/800 s). From this, the instantaneous velocities (v_A and u_A) can be calculated and then the coefficient of restitution can be obtained by the simplified Equation 16.

Figure 33 shows images from the high-speed camera before (a and b in Figure 32a) and after (c) particle impacting the "particle plate". The three panels correspond to particles at a, b and c positions schematically indicated in Figure 32a. The first two panels can be used to determine the instantaneous velocity of particles before impacting on the table and the last panel can be used to determine the instantaneous velocity of particles after impacting on the table. In order to reduce the effect of randomness and ensure the accuracy of the experiments, five particles were collected and each experiment of one kind of particle was repeated ten times. It has been demonstrated that the dropping height has little effect on the COR [125], so a fixed dropping height of 1 m was used in this research. Table 4 summarizes the average value and the standard deviation of COR. No significant differences (at 95% confidence) appeared between the samples. The standard deviation is within acceptable limits, which demonstrates the reliability of the results.
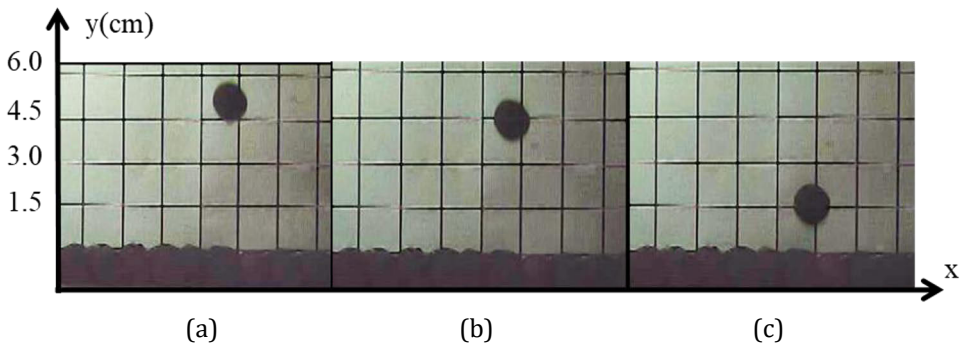

(a)　　　　　　　　　(b)　　　　　　　　　(c)

Figure 33. *Images from the high-speed camera before (a, b) and after (c) particle impacting the table during the measurement of COR, e.g. P-P.*

Table 4 *Measurement results of COR and its standard deviation (σ).*

Contact type	P-P	S-S	C-C	P-Steel	S-Steel	C-Steel
COR (e)	0.42	0.35	0.39	0.62	0.4	0.42
Standard deviation (σ)	0.013	0.030	0.016	0.069	0.015	0.042

(2) Coefficients of static and rolling friction

Figure 32b shows the schematic diagrams related to the determination of static friction between two objects. A sphere is on an inclined surface and is subjected to gravity (m_1g), support force (F_s) and friction force (F_f). The static friction is defined as a trend of relative sliding between two objects in contact, but the objects remain relatively stationary. The measurement device of the coefficient of friction (COF) is shown in Figure 34, which is a semi-automatic system. A transmission mechanism (6 in Figure 34a) is used to move the bottom slider, and then the upper slope (2 in the figure) is lifted by the support rod (3 in the figure). During the test, the inclination angle (θ) of the protractor at the bottom of the device was recorded. The tangent value of θ corresponding to the instant of particle movement represents the coefficient of static friction (μ_s). In order to ensure that particles only slip but do not roll on the upper slope,

particles were glued on a small light plate, the weight of which was negligible. The measurement results of different contact types are shown in Table 5.
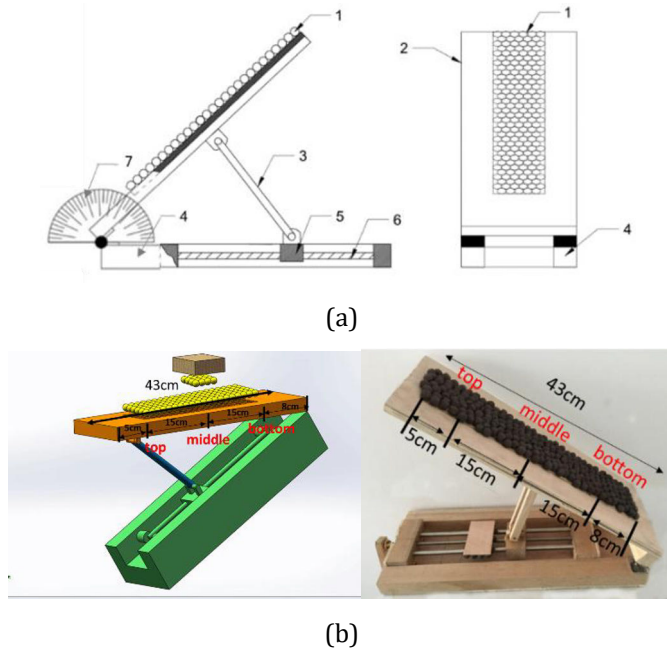

(a)

(b)

Figure 34. Measurement device of COF: main view and left view (a) and three-dimensional representation of device and actual device (b). 1 Particle plate, 2 Upper slope, 3 Support rod, 4 Lower plane, 5 Slider, 6 Transmission mechanism, and 7 Protractor.

Table 5 *Angle and coefficient of static friction, standard deviation (σ) of different contact types.*

Contact type	P-P	S-S	C-C	P-Steel	S-Steel	C-Steel
Angle	33.17	37.25	40.88	19.62	27.36	26.5
μ_s	0.65	0.76	0.87	0.36	0.52	0.5
Standard deviation (σ)	0.022	0.065	0.054	0.013	0.032	0.044

Rolling friction is the force resisting the rotational motion and is usually expressed in terms of a torque. A schematic diagram related to the rolling friction between two objects is given in Figure 32c, where F is the thrust force, and m_2g expresses the gravity force, r is the radius, d is the distance between A and the vertical line through o, while α expresses the inclined angle of the connection of Ao and the vertical line. The calculation principle of the coefficient of rolling friction (μ_r) is based on the conservation of energy due to energy consumption caused by particle rolling. In our work, a direct measurement method was applied for the coefficient of rolling friction of spherical particles (pellet). The particle was put on the slope with angle ($\theta = 30°$) greater than that of the static friction angle of the device (Figure 34) and a high-speed industrial camera recorded the rolling process. Images of the measurement of the coefficient of rolling friction of P-P and P-steel are shown in Figure 35. The initial (v_1) velocity of the particle (panel b in Figure 35) can be calculated by the distance between a

and b, b and c and the final velocities (v_2) can be calculated by the distance between d and e, e and f with the time interval. For ease of calculation, the same time interval (0.05 s) was kept between consecutive images. The calculation principle of the instantaneous velocity is the same as that used in the measurement of the coefficient of restitution: the initial and final velocities of the particles with radius (r) at one segment displacement (L) of the slope were calculated, and the coefficient of rolling friction was given by

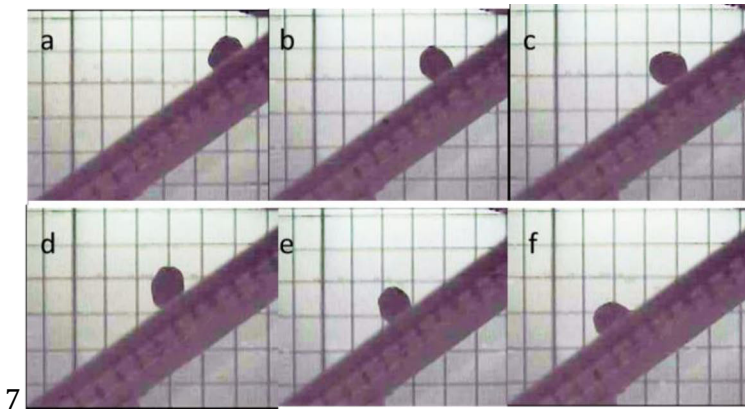$$\mu_r = \frac{[2gL \cdot \sin\theta - (v_2^2 - v_1^2)] \cdot r}{2g \cos\theta \cdot L} \qquad (17)$$

7

Figure 35. *Images of the measurement of the coefficient of rolling friction, where panels a, b and c are used to determine the initial velocities of the particle, and panels d, e and f are used to determine the final velocities.*

As for non-spherical particles (coke and sinter), the values were obtained by comparison of the repose angle of bulk materials in experiments and simulations. A series of DEM simulations of the system with different coefficients of rolling friction were undertaken and the corresponding angle of repose was compared with the experimental ones to determine proper values. The measured coefficient of rolling friction of P-P, C-C and S-S were 0.24, 0.46 and 0.38, respectively.

4.2.2 Validation of DEM parameters

Figure 36 shows a comparison of free surfaces of heaps obtained by simulations and by experiments using pellet, coke and sinter particles. The inserted figures of every graph show the experimental and simulation results of the stable heap. It can be seen that the free surface of the heap in simulations and experiments shows relatively good consistency.

The results demonstrate the validity for the bulk behavior of the parameters estimated in single-particle tests. Thus, single-particle tests constitute a viable option for estimating material and contact parameters in DEM simulation of the blast furnace burden when using the no-slip Hertz–Mindlin contact model. The experimental and simulated results show good consistency, which demonstrates that the measured DEM parameters are accurate enough to be used in

simulations of more complex conditions encountered in different parts of the ironmaking process.
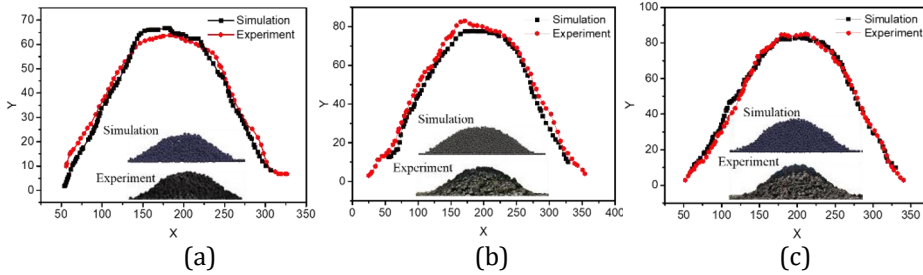

Figure 36. *Comparisons of the free surface of simulated heaps and experimental ones for pellet (a), coke (b) and sinter (c).*

4.3 Modelling of burden descent (Papers III and IV)

4.3.1 Simulation of burden charging

The upper shaft of the BF is a complex packed bed, since it consists of alternative coke and pellet/sinter layers and mixed layers. The porosity distribution or ore-to-coke ratio of the burden layers in the BF plays an important role for the gas distribution and gas-solid two-phase interaction. In the work presented in Paper III and Paper IV, a 2D slot model (cf. Figure 37b) and 3D sector model (cf. Figure 38) of the blast furnace throat were established to simulate the burden distribution during its charging and descent. For the 2D slot model, the BF throat was simplified to a slot with a width of 0.1 m to reduce the computation load, while for the 3D sector model, a 60° (= θ) section of the throat with a radius of 2 m was used, which kept the number of particles reasonable.
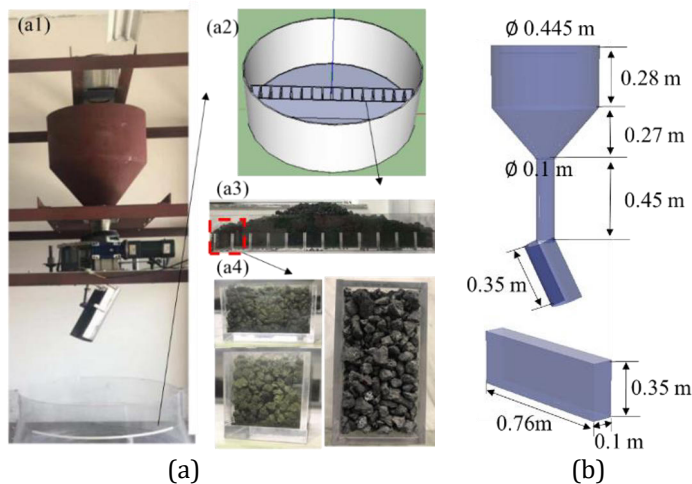

Figure 37. *Physical experimental equipment (a): 1:10 scale model of the charging system and experimental measurement of porosity (a1), installation diagram of measurement equipment at blast furnace throat (a2), formed heap (a3) and three views of a single box full of particles for measuring porosity (a4) and simulation geometry of the charging system with a 2D slot model (b).*

Coke and ore particles were charged from the top into the hopper in random order. After forming a stable bed in the hopper, the exit of the hopper was opened and particles were charged into the blast furnace throat in alternate layers of sinter (pellets) and coke using the rotating chute with a speed of 8 rpm. The particle size and number used in these two simulations are shown in Table 6. In the simulation, spherical particles with adjusted coefficients of rolling friction to consider the effect of the true particle shape were used to represent sinter and coke since spherical particles can reduce the calculation load. Other important charging information is the stockline level (i.e., distance between the burden surface and the lower edge of the distribution device) and the charging program (cf. Table 6). In the simulation of the burden charging, keeping the stockline constant is important to form a stable burden bed. The charging program selected shows resemblance with programs applied in industrial blast furnaces: in particular, 20° corresponds to the center-coke chute angle. One ring of particles was charged for each angle.
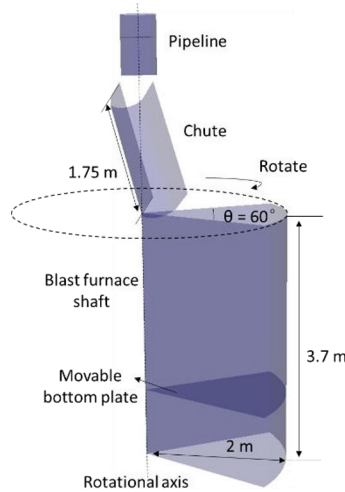
Figure 38. *Geometry of the 3D sector model used in the simulation.*

Table 6 *Burden and charging information of 2D slot and 3D sector throat models in DEM simulation.*

Model	Burden	Size (d_p, mm)	Particle number ($\times 10^3$)	Charging matrix (angle°)	Stockline (m)
2D slot	Sinter	3, 6, 11	57	37, 34, 31	0.24
	Coke	6, 10,15/ 9, 15, 20	32	37, 34, 31, 12	
3D sector	Pellets	11	220	45, 40, 43, 37, 34,	1.25
	Coke	25/40	23/18	45, 40, 43, 37, 34, 20	

4.3.2 2D slot throat model

A. Experimental setup

The radial porosity distribution of a coke layer composed of three particle sizes created by a 1:10 scale pilot model (cf. Figure 37a1) was used to validate the DEM results based on a 2D slot throat model. The general design of this charging system is similar to that of a blast furnace of a steelmaking company in China. It consists of three main parts: a hopper, a rotating chute and a throat made of plexiglass in the model. The mass fractions of small, middle and large cokes were either 10%, 30% and 60% or 20%, 40% and 40%. The charging program applies the chute angles 37°, 34°, 31° and center-coke at 12° with one ring for each angle. To determine the porosity in the arising bed, a simple device was designed (Figure 36a2), which was made of twelve identical small boxes (50 mm × 100 mm × 40 mm) in a large box. The function of the large box is to keep the small boxes unmoved. Every small box has a length of more than six times the maximum particle size and sixteen times the minimum particle size. One small box contains several hundred particles, which means it large enough to make the effect of walls on the estimated porosity small. The device was fixed on the bottom of the throat. When the charging program was applied, the particles fell into the throat and filled the small boxes of the device, simultaneously forming a burden layer (Figure 37a3). The small boxes filled with particles were gently removed from the burden layer (Figure 37a4) to estimate the porosity distribution by the drainage method (cf. Equation 14).

B. Porosity distribution of the burden bed

The simulation process of radial porosity distribution of a coke layer mimics the experimental process. A comparison of simulated and experimental radial porosity distribution of coke layer for the two sets of mass distribution of the size fractions is shown in Figure 39. The DEM results are seen to show general agreement with the experimental findings, but on a more detailed level the results reveal some differences. The porosity in the center and intermediate radial positions of the throat is somewhat smaller in the experiments. Furthermore, it may be concluded that the simulated porosity distribution is more symmetrical and more uniform than the experimental ones for both mass fraction cases. These differences may arise from systematic errors and non-idealities in the experiment. The experimental error bars shown in Figure 39 support this hypothesis. The data also indicates that the mass fraction of different particle sizes has an effect on the radial porosity distribution: the porosity decreases with the increase of the mass fraction of small particles. Despite the small differences, the simulation results are basically consistent with the empirical findings, which demonstrates the validity of the numerical model. This is an important observation for future studies of the dynamics of porosity in the blast furnace based on DEM.

A burden bed with six layers without central coke charging in the blast furnace throat was numerically simulated to investigate the porosity distribution. The burden distribution process is illustrated in Figure 40a, while Figure 40b shows the screenshots of the six burden layers and the particle size distribution. It can be seen that there is an obvious size segregation along the radial direction. Large particles are more easily to gather in the central position

of the furnace throat, as they have higher kinetic energy and are more prone to roll to the bottom of the inclined burden surface, while smaller particles get trapped at or close to the impact point of the burden stream. The uneven distribution of particle size will lead to the differences in the local porosity.
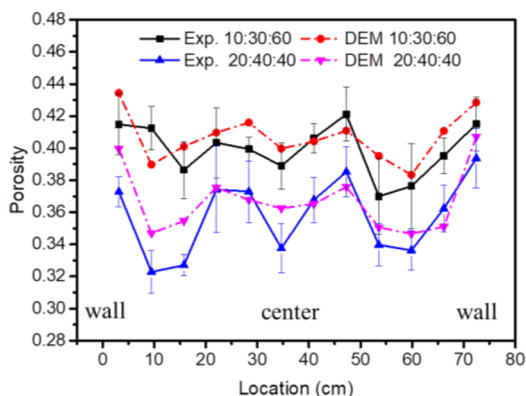

Figure 39. *Comparison of the simulated and experimental radial porosity distribution of coke layer in the BF throat (10:30:60 and 20:40:40 represent the mass fraction of small, middle and large particles).*
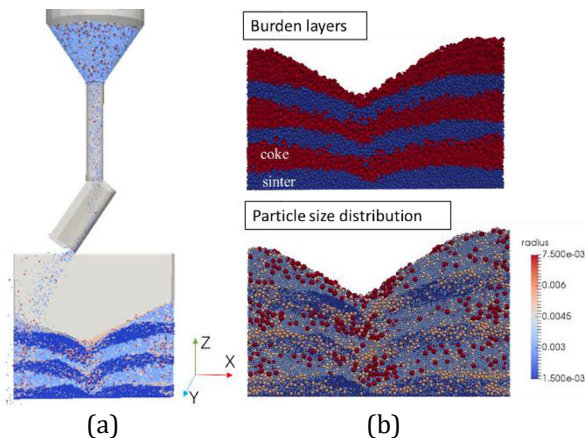

| (a) | (b) |

Figure 40. *Burden distribution process (a), main views of the burden layers (top) and size distribution (bottom) (b).*

The difference of the particle size makes small particles penetrate into the voids of large particles and this phenomenon is more obvious for the mixed layers formed by sinter charged on coke. This can be further confirmed by the coordination number (CON) of particles in the mixed layers shown in Figure 41a, which expresses the average number of particle contacts for a particle. It can be seen that the mixed layer has the maximum value of CON. This is an obvious consequence of a percolation of the smaller sinter particles into the void formed by the larger coke particles. The CON in the sinter layer is also larger than in the coke layer. Figure 41b shows the vertical porosity distribution of the bed in the center, where the ordinate expresses the vertical direction of the shaft from the top to the bottom. The data points enclosed by red squares represent the mixed layers formed by sinter charged on coke, where the porosity is clearly smallest.

The layered structure and the mixing effects caused by particles in different layers lead to a zigzag increase in porosity from the bottom to the top of the BF throat. From the above, it can be concluded that the porosity of the coke layer is larger than that of the ore layer but both have larger porosity than the mixed layers. A large CON indicates small porosity and poor gas permeability.
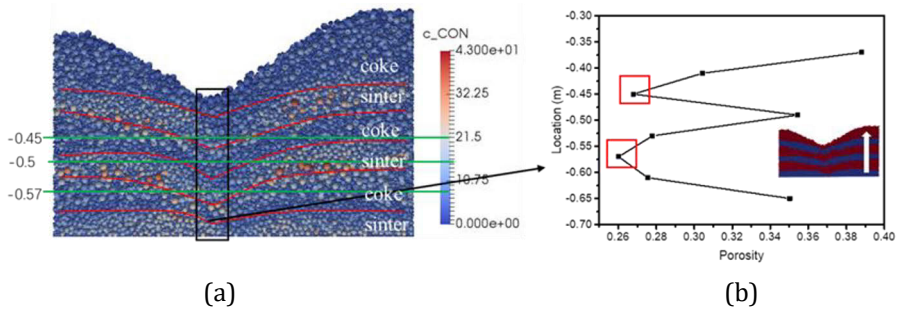

(a)   (b)

Figure 41. Coordinate number of the burden bed (a) and the vertical porosity distribution for the central area (b).

4.3.3 3D sector throat model

A. Study of non-uniform burden descent

A schematic of the DEM simulation process of a 3D slightly down-scaled (throat radius 2 m) blast furnace applied in the work of Paper IV, including burden charging, deleting and descent, is shown in Figure 42. In order to simulate the effect of burden descent, a movable bottom plate is applied, which can be lowered after charging the last ring of each layer to keep a constant stockline level at the moment when charging is triggered. This process was repeated until a sufficient thickness of the original burden bed was formed (cf. subpanel 3 of Figure 42). The arising burden surface can be characterized as an almost flat burden profile. Three kinds of burden descent types were studied in this work, i.e., faster central descent ($V_c > V_w$), uniform descent ($V_c = V_w$) and faster peripheral descent ($V_c < V_w$). After charging, the particles contained in virtual boxes at the bottom of the domain are deleted to realize a burden descent in a quite realistic way. The total thickness (height) of the virtual boxes should meet the requirements of keeping the height of the stockline unchanged at the moments when the charging of a new layer starts. Non-uniform burden descent can be realized by deleting particles in three virtual boxes with different radial extent, as shown schematically in Figure 43. A faster burden local descent was achieved by deleting more particles in the area in question. It should be noted that the box heights applied for the cases of non-uniform descent are different (Δz_c and Δz_w) to delete equal volumes for both cases. The alternating charging and deleting processes were repeated a sufficient number of times until the bed reached a quasi-stationary state, after which the burden distribution was analyzed.

The formed burden bed was divided into ten "virtual boxes" of equal width (0.2 m) in the radial direction. The ore-to-coke mass ratio was calculated by determining the number of coke and pellets particles in each box under the condition that the central point of particles should fall within the box. The height

of each box was chosen to include all the particles in, but not the void above the bed. It should be pointed out that the sector-like domain used in the simulations led to quite few particles near the shaft centerline, so the results for the first box were disregarded.
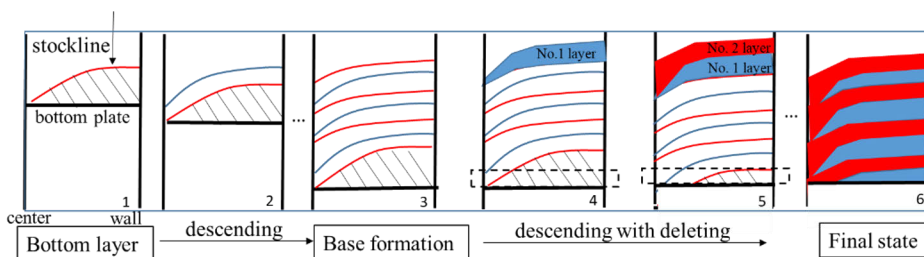

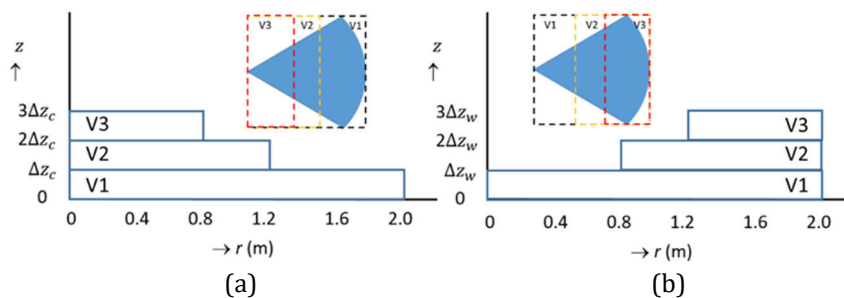**Figure 42.** *Schematic of the simulation process, including burden charging, deleting and descent.*

Figure 43. *The 2D front and top views of virtual boxes used for non-uniform burden descent of $V_c > V_w$ (a) and $V_c < V_w$ (b).*

B. Radial ore-to-coke ratio of burden bed

Figure 44 shows the vertical cross sections of the simulated burden bed for uniform and non-uniform burden descent for the cases where the beds have reached a quasi-stationary state with the charging program (cf. Table 6). During the charging-descending process, a total of eight layers were charged. The different radial distributions of the burden descent rate are seen to yield fundamentally different shapes of the layers. For uniform burden descent (Figure 44b), the burden surface close to the BF wall is flatter than that close to the center. For the cases of non-uniform burden descent, the shapes of the layers change considerably from the top to the bottom of the burden bed.

Figure 45 shows the transient velocity magnitude distribution of the cross section when the burden in the virtual boxes is deleted non-uniformly. For the two kinds of non-uniform burden descent, the instantaneous velocity when the burden starts to descend is about 0.6 m/s. The figure shows the velocity of the burden moments after deleting the particles in the bottom box that spans the whole shaft cross-section (subfigures numbered 1 and 2), the middle box (subfigures 3 and 4) and the top box (subfigures 5 and 6) for the case where the descent rate is larger in the center (Figure 45a) or larger at the wall (Figure 45b). As the particles in the virtual boxes are deleted, the closest overlying particles of the bed first collapse and rapidly descend and the effect is then propagating upwards. The effect also propagates radially, making the whole bed descend.

48

Since the time between the deletions of the particles in the virtual boxes is short, the overall effect is a non-uniform descent of the whole bed.

center   wall center   wall center   wall
            (a)   (b)   (c)
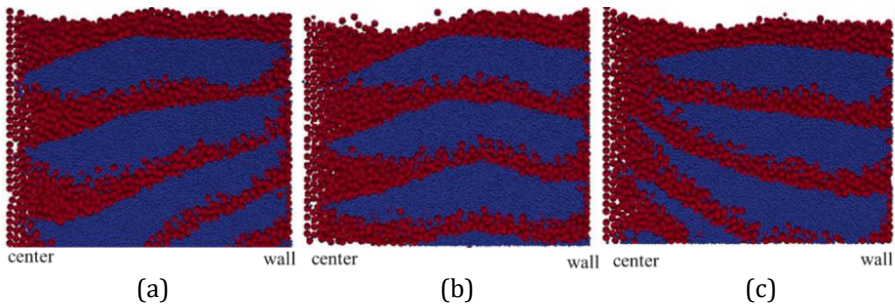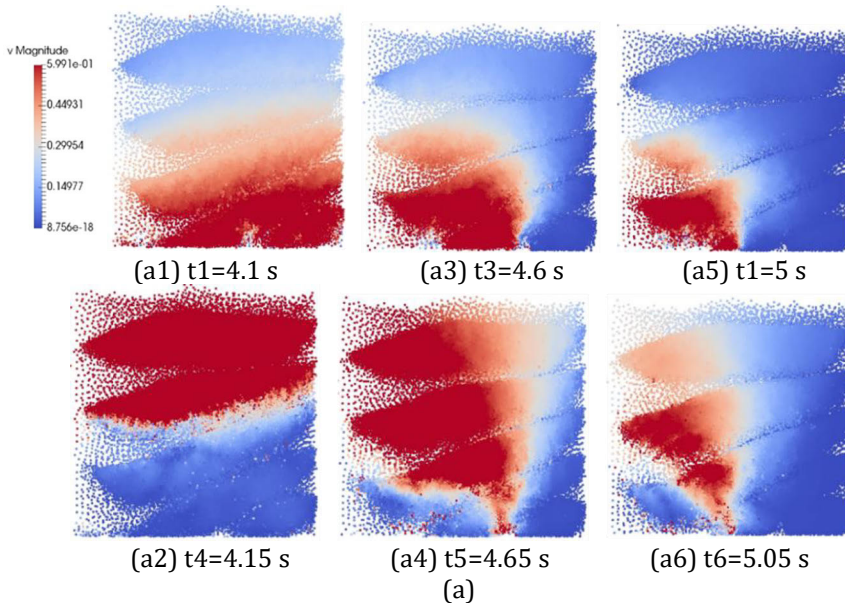
Figure 44. Cross sections of the burden bed in the BF throat for uniform and non-uniform burden descending. Red and blue represent coke and pellets, respectively. $V_c > V_w$ (a), $V_c = V_w$ (b), and $V_c < V_w$ (c).

The radial ore-to-coke mass ratio of the burden bed in the throat for uniform and non-uniform burden descent is shown in Figure 46, where the dashed line represents the overall ore-to-coke ratio based on all particles in the bed. For this specific charging matrix, the maximum of the ore-to-coke ratio occurs roughly halfway between the furnace center and the wall, and the maximum point is seen to be shifted towards the point where the descent rate is higher. At the center and the wall, the ratio is relatively small, and decreases at the points where the descent rate is low and increases where it is high. This effect is more clearly seen for the case with $V_c > V_w$. Dong et al. [94] explained this by the fact that the angle of repose is smaller for ore than coke, causing more ore particles to be spread from the impact point. In fact, both coke and ore particles will slide or roll along the increased slope caused by non-uniform burden descent, simultaneously leading to more percolation of ore (with smaller size) into the voidage between large coke particles, which serves to increase the ore-to-coke ratio.

(a1) t1=4.1 s   (a3) t3=4.6 s   (a5) t1=5 s

(a2) t4=4.15 s   (a4) t5=4.65 s   (a6) t6=5.05 s
                              (a)

(b1) t1=4.1 s   (b3) t3=4.6 s   (b5) t1=5 s

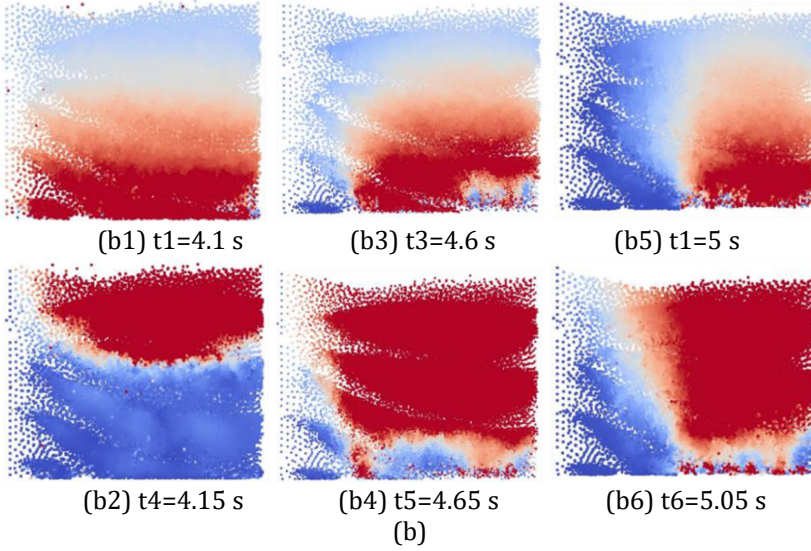(b2) t4=4.15 s   (b4) t5=4.65 s   (b6) t6=5.05 s

(b)

Figure 45. Velocity distribution of particles for non-uniform burden descent at times after deleting particles in the virtual boxes for $V_c > V_w$ (a), $V_c < V_w$ (b). Subfigures 1, 3 and 5 show the velocity distribution when the deletion of burden starts in the virtual boxes, while subfigures 2, 4 and 6 show the velocity distribution 0.05 s later when the whole burden descends.
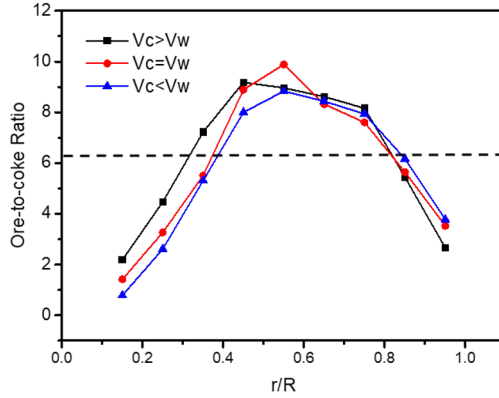
Figure 46. Radial ore-to-coke mass ratio of the burden bed with uniform and non-uniform burden descent. The overall ore-to-coke ratio is indicated by a horizontal dashed line.

The difference between the pellets and coke size is one of the most important factors influencing the radial ore-to-coke ratio because of the percolation of ore particles. To further study this effect, a burden bed with larger coke size (40 mm instead of 25 mm, cf. Table 6) was simulated using the same charging matrix. In order to facilitate a comparison between the results despite this change, the ore-to-coke ratio was normalized by

$$S = \frac{\left(\frac{o}{c}\right)_i - \left(\frac{o}{c}\right)_{tot}}{\left(\frac{o}{c}\right)_{tot}} = \frac{\left(\frac{o}{c}\right)_i}{\left(\frac{o}{c}\right)_{tot}} - 1 \qquad (18)$$

where $\left(\frac{O}{C}\right)_i$ is the ore-to-coke ratio at a point i on the radius, $\left(\frac{O}{C}\right)_{tot}$ is the overall ore-to-coke ratio and S is the normalized ore-to-coke ratio.

When the particle size ratio, $\alpha = d_p/d_c$, decreases, where d_p and d_c respectively represent the diameters of the pellets and coke, more (smaller) pellets particles will permeate into the voidage between the coke particles. Figure 47 shows the normalized radial ore-to-coke ratio of small ($\alpha = 0.44$) and large ($\alpha = 0.275$) coke for beds with uniform and non-uniform burden descent. It can be seen that the over-all trend of the normalized ore-to-coke ratio is similar for the two coke sizes. Compared with the small coke, the large coke increases the ore-to-coke ratio near the center and decreases it near the wall.

Figure 48 shows the change of the radial ore-to-coke ratio during burden descent. Charging only four layers overestimates the share of ore in the intermediate part of the radius ($r/R \approx 0.5$). Including more layers in the analysis stabilizes the results: the curves for the six- and eight-layer beds are almost identical. This phenomenon is more obvious for the case with $V_c < V_w$. Thus, one may conclude that beds formed by six layers or more (charged on the base layer) represent the quasi-stationary state of the bed, irrespective of the type of burden descent.

(a)   (b)   (c)
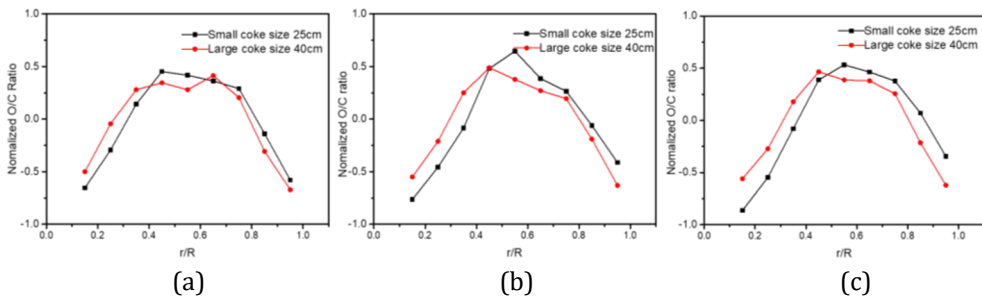
Figure 47. *Comparison of the normalized radial ore-to-coke ratio for beds of small and large coke sizes. $V_c > V_w$ (a), $V_c = V_w$ (b), and $V_c < V_w$ (c).*

(a)   (b)   (c)
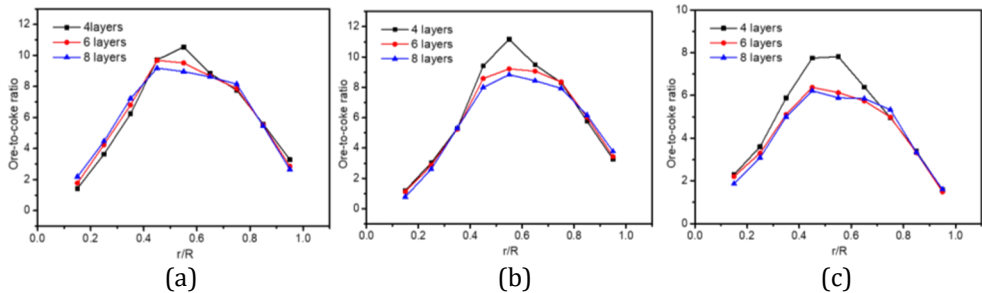
Figure 48. *Radial distribution of the ore-to-coke ratio of a bed charged with an increasing number of layers (on the base layer), with small coke for $V_c > V_w$ (a), $V_c < V_w$ (b), and large coke for $V_c < V_w$ (c).*

The 3D sector throat model was successfully established to help to understand the behavior of burden descent in the upper part of the blast furnace. Compared to the 2D slot throat model, 3D model gives more information about the burden distribution and the results more closely reflect the actual conditions

of the upper part of the blast furnace. The findings are expected to be helpful for the design of charging programs under different states of operation of the furnace, and also for a more accurate interpretation of signals from profile meters. The results may also be used to make more accurate assumptions concerning the behavior of the burden in mathematical models that the motion of individual particles.

4.4 Gas distribution at burden charging (Paper V)

4.4.1 System considered for CFD-DEM modelling

The gas temperature and flow in the upper part of the blast furnace were studied computationally by CFD-DEM simulation using EDEM-ANSYS Fluent in a model which also considered thermal aspects. The numerical solution used about 35,000 grid points and time steps of $1.5 \cdot 10^{-5}$ s for the particle updates and $5 \cdot 10^{-4}$ s for the gas flow. To simplify the treatment and to reduce the computational burden, a 3D sector model of one fourth of a small cylindrical shaft (Figure 49a) was considered with periodic boundary conditions at the plane "walls". Intermittent charging of two types of particles, coke and pellets, at "ambient" temperature (300 K) was applied onto the surface of the burden bed that descends due to spontaneous outflow of it through a slot in periphery of the lower part of the domain. The slot size was adjusted so a steady outflow at a suitable speed was established. Within the virtual boxes seen in the top part of Figure 49a, and in detail in Figure 49b, spherical particles of two types, pellets (d_p = 0.015 m) and coke (d_c = 0.060 m) were generated, at roughly equal volumes (which resembles the conditions in the blast furnace). Coke was charged closer to the center and pellets closer to the wall, which corresponds to a common charging pattern in the blast furnace. Gas of a higher temperature (800 K) was blown into the system at the bottom of the domain at a given constant velocity (+ 0.5 m/s), creating a counter-current system that resembles the one encountered in the blast furnace shaft, where the ascending gas heats the descending burden. The arising burden distribution is expected to lead to a stronger central gas flow and a higher gas temperature due to the higher permeability of coke.

The system was simulated to a quasi-stationary state by first generating a layered bed and then applying alternatingly charging of coke and pellet layers. The time between charging was adjusted so the burden surface level (stockline) was kept at a constant vertical level (z = 2.5 m) when charging was triggered. The gas pressure at the top (i.e., outlet) was fixed at 2 bar. To make the particle simulation feasible, the burden descent rate must be much faster in the simulated system than in the industrial counterpart. To consider this in the energy balance to make the thermal conditions similar in the two systems, the gas heat capacity was strongly elevated. This was made instead of increasing the gas flow rate accordingly to avoid an excessive gas drag and a potential fluidization of the particles. The thermal flow ratio, i.e., the ratio between the heat capacity flows of burden and gas, was set to 0.8, which is a common value in blast furnaces. Furthermore, to enhance the heat transfer due to the short

residence time of the burden in the simulated domain, the gas-burden heat transfer coefficient and thermal conductivity of the solid phase were increased by a large factor (200).
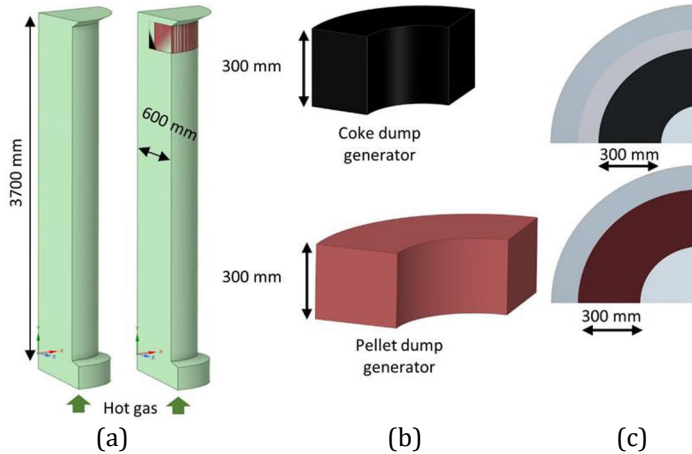

Figure 49. *Isometric view of the domain of the model with particles generated at the top and gas entering at the bottom. A slot in the bottom sidewall creates an outflow of particles (a). Domain within which particles are generated (b) and top view (c)*

4.4.2 Gas temperature and flow dynamics

Figure 50 shows a view of the thermal and flow conditions of the system in quasi-steady state seen through one of the planes with periodic boundary conditions. The bed temperature (Figure 50a) is seen to rise from the initial temperature (dark blue) to eventually approach the temperature of the injected gas (800 K), substantially faster in the center than at the wall. It is also interesting to note that the pellets are heated more rapidly despite their considerable higher density, which shows the role of the larger area-to-volume ratio $A_p/V_p = 6/d_p$ and also the lower specific heat capacity. Lower down in the shaft the differences become less clear due to pellet percolation and radial motion of the descending burden.
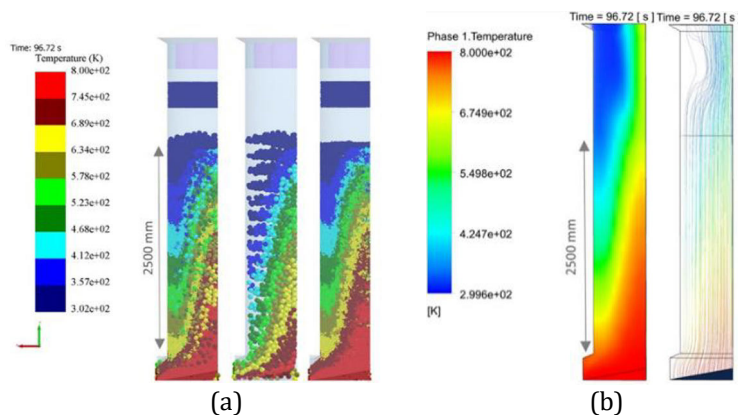

Figure 50. *Temperature of the system in quasi-steady state seen through the plane with periodic boundary conditions. (a) Full bed (left), coke particles (middle), and pellet particles (right). (b) Gas temperature distribution (left) and streamlines (right).*

The gas flow (expressed by streamlines) and temperature (after a coke dump) are depicted in Figure 50b. The higher gas permeability of the coke layers yields a strong center-gas flow, which largely avoids the dense pellet layers formed at the wall. The gas temperature leaving the bed is about 600 K in the center, but only slightly above the burden temperature at the wall.

To illustrate the dynamic conditions in the upper part of the domain, the changes of the gas temperature and velocity were considered from the perspective of time and space. Figure 51a illustrates the gas streamlines at $t = 88$ s with a plane at $z = 2.8$ m, which is 0.1-0.3 m above the burden surface. The gas flow at different radial positions can be studied by dividing the plane into eight concentric "rings" (cf. in Figure 51) with equal radial increment (0.075 m) and at each vertical level an average of the temperatures was taken, excluding 5° of the sector at the two symmetry planes due to disturbances caused by the periodic boundary conditions.
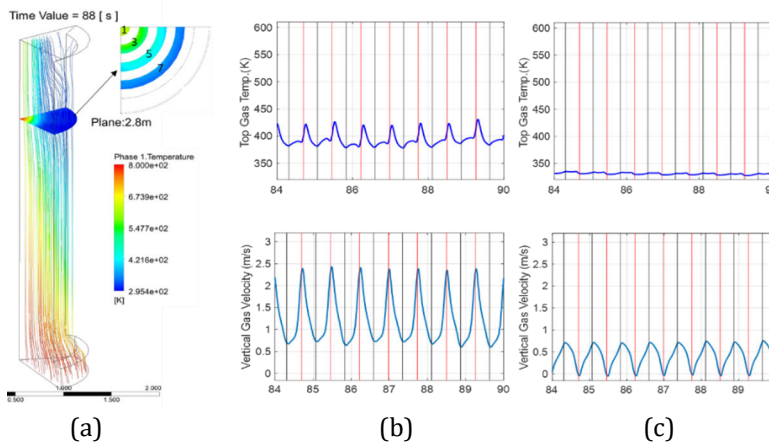

(a)   (b)   (c)

Figure 51. *Gas streamlines at t = 88 s with a plane at z = 2.8 m (a), mean gas temperature (upper) and gas velocity (lower) of Ring 3 (b) and Ring 7 (c) for a period of 6 s.*

The upper panels of Figure 51b and 51c depict the mean values of the gas temperatures in Rings 3 and 7 for a time interval of six seconds. Vertical black and red lines indicate the moment when dumps of coke and pellets have been charged onto the burden surface. The figure clearly illustrates the large temperature difference between the center and the wall regions. The temperature of Ring 3 (Figure 51b, upper panel), which varies around 400 K (130 °C), shows fundamentally different dynamics and larger changes: a main temperature drop (of about 45-50 K) is experienced after the pellet dump, while the coke dump leads to practically no temperature change. The "recovery" after the temperature drop that follows the pellet dump overrides the cooling effect of the coke dump. Even though most parts of it enters the wall region, the pellet dump has a large effect due to gas redistribution, which forces gas from the periphery towards the center. Ring 7 (Figure 51c, upper panel) shows minor temperature changes at charging since the "driving force" for the heat transfer is little because the temperature difference between the gas and burden is small (only about 30 K). The lower panels of Figure 51b and 51c depict the mean of the vertical gas velocities in the rings. Ring 3 shows the strong gas flow in the center,

with velocities ranging between 0.5 m/s and 2.5 m/s. The velocity is seen to be primarily affected by the pellet dumps, but also by the coke dumps: as the dumps enters the burden surface, the velocity spikes. Ring 7 shows the lowest gas flow rates at the pellet dumps, which "clog" the wall region temporarily.

Figure 52 illustrates the radial distribution of the gas temperature and vertical velocity component on the z = 2.8 m level during a charging cycle (t = 86.6 s, 86.8 s, 87.0 s, 87.2 s and 87.4 s). The temperature changes in the different parts (Figure 52a) are seen to be small in the center due to a low thermal flow ratio and at the wall due to a small temperature difference between the gas and burden. Even though the shaft studied in this work is strongly down-scaled and the burden distribution is simplified, the arising radial temperature distribution resembles profiles measured by above-burden probes in operating blast furnaces. By contrast, the (vertical component of the) gas velocity (Figure 52b), shows dramatic changes. The pellet dump that enters at $t \approx 87.0$ s fundamentally changes the distribution, shifting the gas from the wall region to the center. This brings about a large change of the mean top gas temperature, even though the gas temperatures at the different radial points change much less (cf. Figure 52a), as discussed in Paper V.
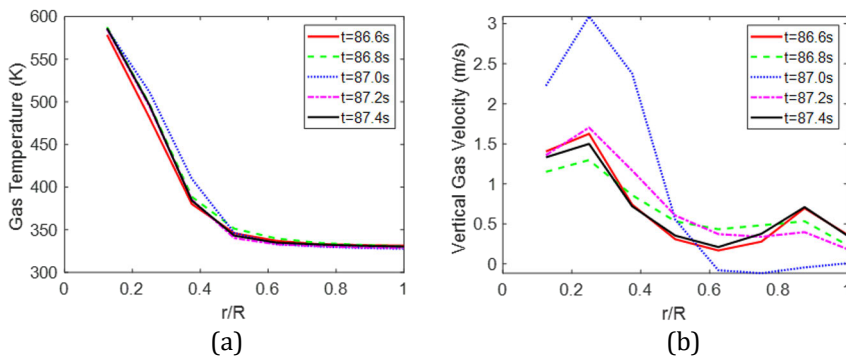
Figure 52. *Radial distribution of gas temperature (a) and vertical velocity component (b) above the burden surface (z = 2.8 m) during a charging cycle, starting at t = 86.6 s and ending at t = 87.4 s with time steps of 0.2 s.*

Overall, the dynamics of the system were found to be complex since the gas temperature exhibits changes due to heat transfer and mixing of gas from different regions. Also the gas velocity showed a complex evolution in time, but in agreement with the scarce findings from measuring campaigns in real furnaces. The results of the study have shed more light on the complex and dynamic operation of the upper part of the blast furnace shaft and provided an explanation of how the measurements above the burden surface are affected by the intermittent charging.

5 Conclusions

As a complex multiphase system, the blast furnace exhibits many challenges in the operation and control due to incomplete information about the internal state and a lack of understanding of the interrelation between variables in the process. In the upper part of the furnace, only two phases (solids and gas) are present, but the radial distribution of gas and burden is still not understood sufficiently well, which limits the success of control actions to achieve a high efficiency and stable operation state. Research on the distribution of burden and gas by local modelling and small-scale experiments yield a better understanding of the phenomena and the conditions in the blast furnace shaft. The thesis presented a study of the voidage distribution in particle heaps to determine appropriate parameters for DEM models, which were applied to analyze the upper part of the burden bed in the blast furnace by DEM simulation. Small scale experiments were used to support the findings and to validate the numerical models.

 A better understanding of granular systems is useful for designing and optimizing industrial processes. To study the properties of granular systems of relevance in ironmaking, three particle shapes were selected to empirically study the packing of particles of a heap by experiment and DEM. The effect of the coefficient of rolling friction on the repose angle and porosity distribution of the particle heap is relatively small compared to the effect of coefficient of static friction. There is a minimum value of the average porosity of the heap with a change of sphericity φ (found at about $\varphi = 0.85$). A comparison of the porosity distribution in experiments and simulations demonstrated that the DEM model established based on findings for the particle heaps can provide a relatively accurate prediction of the porosity distribution in systems of relevance for ironmaking.

In order to further guarantee the accuracy of the burden flow predictions in blast furnace by DEM, some key physical parameters of the main burden materials were measured directly or indirectly. A calibration of parameters was undertaken by a comparison of the resulting free surface of conical heaps in simulations and experiments. Means of measuring of coefficient of restitution, coefficient of rolling and static friction between particle and particle and between particle and steel plate were proposed and successfully applied to obtain the value with small-scale laboratory devices. The experimental and calculated results showed good consistency, which demonstrated that the "measured" DEM parameters are accurate enough to be used in simulations of industrial systems.

A 2D slot throat model and a 3D sector throat model with a bell-less burden charging system were established to study the burden layers in the BF throat at burden charging and descent. A 1:10 scale bell-less charging system was designed and used for experiments. The porosity of the coke layer is larger than that of the ore layer but both have larger porosity than the mixed layers. A numerical method to study the effect of non-uniform burden descending was proposed, where particles were deleted in three virtual boxes with different radial extent in the lower end of the simulated domain. The results showed that the radial ore-to-coke ratio decreases at points where the descent rate is low and

increases where it is high, and this effect is more clearly seen for the case with $V_c > V_w$.

Finally, the intermittent charging and continuous descent of burden, and the simultaneous ascent of gas through the particle bed were simulated with a combined CFD-DEM model. Special attention was paid to the conditions of the gas above the burden surface, analyzing its overall temperature and the temperature and velocity at different radial positions. A main temperature drop (of about 45-50 K) is experienced after the pellet dump and forces gas from the periphery towards the center, while the coke dump leads to practically no temperature change. The model captures the complex interaction between the solid and gas flows, which affects the radial temperature distribution due to heat transfer and gas redistribution, and provides new information about the conditions in the upper shaft and the complex dynamic process in this part of the blast furnace.

6 Future work

This thesis has mainly focused on developing DEM model of particle heaps, measurement of DEM parameters of common burden materials in ironmaking, DEM modelling of burden charging and descent, as well as CFD-DEM modelling of the thermal and flow conditions in the upper shaft under intermittent charging. Even though the above analysis step by step has revealed factors influencing the micro and macro properties of particle heap and burden layers and, further, has provided a more detailed view of how charging affects the gas flow in the upper part of the shaft, there are still several open issues to be studied.

The finding of the effect of burden descent on the layered burden are interesting but the present simulations were limited to the top region of the throat of a small blast furnace. Future work should address the problem in larger scale, extending the domain to the part where the shaft diameter increases, and also include the effect of the cohesive zone. This will give a more realistic view of the true conditions. Furthermore, different and more complex charging programs should be studied, possibly also relating the burden descent rate to the local ore-to-coke ratio.

The CFD-DEM model developed applied a simplified burden charging program and the furnace diameter was small. Future work should consider more realistic charging programs for a system of larger extent, particularly in the radial direction. The computational analysis should be complemented by small-scale experiments with stagnant or moving particle beds with simultaneous gas flow for model validation. In addition, CFD-DEM simulations considering both physical and chemical conditions are needed to assess the overall performance of the shaft and to study the factors influencing burden descent and gas flow patterns in the shaft.

References

[1] A. Orth, N. Anastasijevic, H. Eichberger, Low CO_2 emission technologies for iron and steelmaking as well as titania slag production, Minerals Engineering, 20 (2007) 854-861.

[2] S. Ueda, S. Natsui, H. Nogami, J.I. Yagi, T. Ariyama, Recent progress and future perspective on mathematical modeling of blast furnace, ISIJ International, 50 (2010) 914-923.

[3] X. Dong, A.B. Yu, J.I. Yagi, P. Zulli, Modelling of multiphase flow in a blast furnace: recent developments and future work, ISIJ International, 47 (2007) 1553-1570.

[4] Y. Yang, Y. Yin, D.C. Wunsch, S. Zhang, X. Chen, X. Li, S. Cheng, M. Wu, K. Liu, Development of blast furnace burden distribution process modeling and control, ISIJ International, 57 (2017) 1350-1363.

[5] P. Richard, M. Nicodemi, R. Delannay, P. Ribière, D. Bideau, Slow relaxation and compaction of granular systems, Nature Materials, 4 (2005) 121-128.

[6] H. Jaeger, S. Nagel, R. Behringer, Granular solids, liquids, and gases, Reviews of Modern Physics, 68 (1996) 1259-1273.

[7] J. Duran, R.P. Behringer, Sands, Powders, and Grains: An Introduction to the Physics of Granular Materials, Physics Today, 54 (2001) 63-64.

[8] B. Kou, Y. Cao, J. Li, C. Xia, Z. Li, H. Dong, A. Zhang, J. Zhang, W. Kob, Y. Wang, Granular materials flow like complex fluids, Nature, 551 (2017) 360-363.

[9] C.J. Coetzee, Calibration of the discrete element method and the effect of particle shape, Powder Technology, 297 (2016) 50-70.

[10] Z.Y. Zhou, R.P. Zou, D. Pinson, A.B. Yu, Angle of repose and stress distribution of sandpiles formed with ellipsoidal particles, Granular Matter, 16 (2014) 695-709.

[11] R. Guises, J. Xiang, J.-P. Latham, A. Munjiza, Granular packing: numerical simulation and the characterisation of the effect of particle shape, Granular Matter, 11 (2009) 281-292.

[12] J. Theuerkauf, P. Witt, D. Schwesig, Analysis of particle porosity distribution in fixed beds using the discrete element method, Powder Technology, 165 (2006) 92-99.

[13] J.Q. Gan, A.B. Yu, Z.Y. Zhou, DEM simulation on the packing of fine ellipsoids, Chemical Engineering Science, 156 (2016) 64-76.

[14] Y.C. Zhou, B.D. Wright, R.Y. Yang, B.H. Xu, A.B. Yu, Rolling friction in the dynamic simulation of sandpile formation, Physica A Statistical Mechanics & Its Applications, 269 (1999) 536-553.

[15] J. Lee, H.J. Herrmann, Angle of Repose and Angle of Marginal Stability: Molecular Dyanmics of Granular Particles, Journal of Physics A General Physics, 26 (1992) 373.

[16] D.M. Mueth, G.F. Debregeas, G.S. Karczmar, P.J. Eng, S.R. Nagel, H.M. Jaeger, Signatures of granular microstructure in dense shear flows, Nature, 406 (2000) 385-389.

[17] M. Geerdes, R. Chaigneau, I. Kurunov, O. Lingiardi, J. Ricketts, Modern Blast Furnace Ironmaking, 3rd ed., IOS Press, Netherland, 2015.

[18] X.B. Yu, Y.S. Shen, Modelling of blast furnace with respective chemical reactions in coke and ore burden layers, Metallurgical and Materials Transactions B, 49 (2018) 2370-2388.

[19] Y.W. Yu, H. Saxén, Particle flow and behavior at bell-less charging of the blast furnace, Steel Research International, 84 (2013) 1018-1033.

[20] Y. Xu, J. Xu, C. Sun, K. Ma, C. Shan, L. Wen, S. Zhang, C. Bai, Quantitative comparison of binary particle mass and size segregation between serial and parallel type hoppers of blast furnace bell-less top charging system, Powder Technology, 328 (2018) 245-255.

[21] M. Riddle, P. Whitfield, Design and operation of a Gimbal Top distribution system for ironmaking plants, Ironmaking & Steelmaking, 34 (2007) 221-224.

[22] W.R. Ketterhagen, J.S. Curtis, C.R. Wassgren, A. Kong, P.J. Narayan, B.C. Hancock, Granular segregation in discharging cylindrical hoppers: A discrete element and experimental study, Chemical Engineering Science, 62 (2007) 6423-6439.

[23] S. Wu, M. Kou, J. Xu, X. Guo, K. Du, W. Shen, J. Sun, DEM simulation of particle size segregation behavior during charging into and discharging from a Paul-Wurth type hopper, Chemical Engineering Science, 99 (2013) 314-323.

[24] Y. Xu, J. Xu, Z. Liao, Y. Pei, L. Gao, C. Sun, M. Kou, L. Wen, DEM study on ternary-sized particle segregation during the sinter burden charging process, Powder Technology, 343 (2019) 422-435.

[25] C.M. Dury, G.H. Ristow, J.L. Moss, M. Nakagawa, Boundary Effects on the Angle of Repose in Rotating Cylinders, Physical Review E Statistical Physics Plasmas Fluids & Related Interdisciplinary Topics, 57 (1997) 4491-4497.

[26] J.T. Carstensen, P.C. Chan, Relation between particle size and repose angles of powders, Powder Technology, 15 (1976) 129-131.

[27] M. Alizadeh, A. Hassanpour, M. Pasha, M. Ghadiri, A. Bayly, The effect of particle shape on predicted segregation in binary powder mixtures, Powder Technology, 319 (2017) 313-322.

[28] E. Mousa, D. Senk, A. Babich, H.W. Gudenau, Influence of nut coke on iron ore sinter reducibility under simulated blast furnace conditions, Ironmaking & Steelmaking, 37 (2013) 219-228.

[29] E. Mousa, D. Senk, A. Babich, Reduction of Pellets-Nut Coke Mixture under Simulating Blast Furnace Conditions, Steel Research International, 81 (2010) 706-715.

[30] K.V. Senthil, M. Santhanam, Particle packing theories and their application in concrete mixture proportioning: A review, Indian Concrete Journal, 77 (2003) 1324-1331.

[31] Z.Y. Zhou, R.P. Zou, D. Pinson, A.B. Yu, Dynamic Simulation of the Packing of Ellipsoidal Particles, Industrial & Engineering Chemistry Research, 50 (2011) 287–291.

[32] D. Bideau, A. Hansen, Disorder and granular media, Random Materials & Processes, (1993).

[33] A. Mehta, R.W. Cahn, Granular Matter: An Interdisciplinary Approach, Physics Today, 48 (2008) 91-91.

[34] J. Finney, Random packings and the structure of simple Liquids. I. The geometry of random close packing, Proceedings of the Royal Society of London, 319 (1970) 495-507.

[35] L.F. Liu, Z.P. Zhang, A.B. Yu, Dynamic simulation of the centripetal packing of mono-sized spheres, Physica A Statistical Mechanics & Its Applications, 268 (1999) 433-453.

[36] R.Y. Yang, R.P. Zou, A.B. Yu, Computer simulation of the packing of fine particles, Phys Rev E Stat Phys Plasmas Fluids Relat Interdiscip Topics, 62 (2000) 3900-3908.

[37] T. Gröger, A. Katterfeld, On the numerical calibration of discrete element models for the simulation of bulk solids, Computer Aided Chemical Engineering, 21 (2006) 533-538.

[38] D.B. Hastie, A.P. Grima, P.W. Wypych, Validation of particle flow through a conveyor transfer spoon via particle velocity analysis, in: 2nd International Conference and Exhibition on Storage, Handling and Transporting Bulk, 2008.

[39] H. Kruggel-Emden, E. Simsek, S. Rickelt, S. Wirtz, V. Scherer, Review and extension of normal force models for the Discrete Element Method, Powder Technology, 171 (2007) 157-173.

[40] F.P.D. Maio, A.D. Renzo, Analytical solution for the problem of frictional-elastic collisions of spherical particles using the linear model, Chemical Engineering Science, 59 (2004) 3461-3475.

[41] H. Kruggel-Emden, S. Wirtz, V. Scherer, A study on tangential force laws applicable to the discrete element method (DEM) for materials with viscoelastic or plastic behavior, Chemical Engineering Science, 63 (2008) 1523-1541.

[42] D. Höhner, S. Wirtz, V. Scherer, Experimental and numerical investigation on the influence of particle shape and shape approximation on hopper discharge using the discrete element method, Powder Technology, 235 (2013) 614-627.

[43] J.R. Williams, A.P. Pentland, Superquadrics and modal dynamics for discrete elements in interactive design, Engineering Computations, 9 (1992) 115-127.

[44] X.L. Deng, R.N. Davé, Dynamic simulation of particle packing influenced by size, aspect ratio and surface energy, Granular Matter, 15 (2013) 401-415.

[45] D. Höhner, S. Wirtz, V. Scherer, A numerical study on the influence of particle shape on hopper discharge within the polyhedral and multi-sphere discrete element method, Powder Technology, 226 (2012) 16–28.

[46] D. Höhner, S. Wirtz, V. Scherer, A study on the influence of particle shape and shape approximation on particle mechanics in a rotating drum using the discrete element method, Powder Technology, 253 (2014) 256-265.

[47] D. Höhner, S. Wirtz, V. Scherer, A study on the influence of particle shape on the mechanical interactions of granular media in a hopper using the Discrete Element Method, Powder Technology, 278 (2015) 286-305.

[48] J.F. Ferellec, G.R. Mcdowell, A simple method to create complex particle shapes for DEM, Geomechanics & Geoengineering, 3 (2008) 211-216.

[49] H. Wadell, Volume, Shape, and Roundness of Quartz Particles, The Journal of Geology, 43 (1935) 250-280.

[50] A. Khalili, M. Matyka, R. Malek Mohammadi, J. Weise, M.M.M. Kuypers, Porosity variation within a porous bed composed of multisized grains, Powder Technology, 338 (2018) 830-835.

[51] A.B. Yu, N. Standish, Estimation of the porosity of particle mixtures by a linear-mixture packing model, Industrial & Engineering Chemistry Research, 30 (1991) 1372-1385.

[52] G.E. Mueller, A simple method for determining sphere packed bed radial porosity, Powder Technology, 229 (2012) 90-96.

[53] G.E. Mueller, A modified packed bed radial porosity correlation, Powder Technology, 342 (2019) 607-612.

[54] T. Nikola, J.A.C. Gallas, P.S. Thorsten, Nonuniformities in the angle of repose and packing fraction of large heaps of particles, Physical Review Letters, 109 (2012) 128001.

[55] C.R.A. Abreu, F.W. Tavares, M. Castier, Influence of particle shape on the packing and on the segregation of spherocylinders via Monte Carlo simulations, Powder Technology, 134 (2003) 167-180.

[56] H. Tangri, Y. Guo, J.S. Curtis, Packing of Cylindrical Particles: DEM Simulations and Experimental Measurements, Powder Technology, 317 (2017) 72-82.

[57] H. Delmas, G.F. Froment, A simulation model accounting for structural radial nonuniformities in fixed bed reactors, Chemical Engineering Science, 43 (1988) 2281-2287.

[58] P. Kondelik, J. Horak, J. Tesarova, Heat and Mass Transfer in Heterogeneous Catalysis. Variation of Local Void Fraction in Randomly Packed Beds of Equilateral Cylinders, Industrial & Engineering Chemistry Process Design & Development, 7 (1968) 29-51.

[59] D. Müller, E. Fimbinger, C. Brand, Algorithm for the determination of the angle of repose in bulk material analysis, Powder Technology, 383 (2021) 598-605.

[60] Y.C. Zhou, B.H. Xu, A.B. Yu, P. Zulli, Numerical investigation of the angle of repose of mono-sized spheres, Physical Review E, 64 (2001) 021301.

[61] B.B. Dai, T.Q. Li, L.J. Deng, J. Yang, W.H. Yuan, Fabric effect on the angle of repose in granular materials, Powder Technology, 400 (2022) 117256.

[62] I.S.I.O. Japan, Blast Furnace Phenomena and Modelling, Springer Netherlands, 1987.

[63] J. Hinnelä, H. Saxén, F. Pettersson, Modeling of the blast furnace burden distribution by evolving neural networks, Industrial & Engineering Chemistry Research, 42 (2003) 2314-2323.

[64] D. Fojtik, J. Tuma, P. Faruzel, Computer modelling of burden distribution in the blast furnace equipped by a bell-less top charging system, Ironmaking & Steelmaking, (2021) 1-13.

[65] L. Król, M. Krzaklewski, T. Olek, W. Wozniacki, Identification of burden distribution parameters in shaft and throat of the blast furnace, Steel Research, 59 (1988) 146-152.

[66] S. Liu, Z. Zhou, K. Dong, A. Yu, D. Pinson, J. Tsalapatis, Numerical Investigation of Burden Distribution in a Blast Furnace, Steel Research International, 86 (2015) 651-661.

[67] W. Rankin, P. Roller, The measurement of void fraction in beds of granulated iron ore sinter feed, Transactions of the Iron and Steel Institute of Japan, 25 (1985) 1016-1020.

[68] C. Li, T. Honeyands, D. O'Dea, R. Moreno-Atanasio, DEM study on size segregation and voidage distribution in green bed formed on iron ore sinter strand, Powder Technology, 356 (2019) 778-789.

[69] J. Duan, W. Zhang, Research on the blast furnace charge position Ttracking based on machine learning regression model, in: 2018 10th International Conference on Modelling, Identification and Control (ICMIC), 2018.

[70] H. Saxén, M. Nikus, J. Hinnelä, Burden distribution estimation in the blast furnace from stockrod and probe signals, Steel Research, 69 (1998) 406-412.

[71] T. Yamamoto, T. Shokyu, H. Kanoshima, Y. Hayashi, K. Tamura, T. Takahashi, Development of monitoring system for lumpy and cohesive zones in the blast furnace, ISIJ International, 22 (2006) 774-781.

[72] J. Hinnelä, H. Saxén, Neural network model of burden layer formation dynamics in the blast furnace, ISIJ International, 41 (2001) 142-150.

[73] P. Zhou, P.Y. Shi, Y.P. Song, K.L. Tang, D. Fu, C. Zhou, Evaluation of burden descent model for burden distribution in blast furnace, Journal of Iron and Steel Research International, 23 (2016) 765-771.

[74] V.R. Radhakrishnan, K.M. Ram, Mathematical model for predictive control of the bell-less top charging system of a blast furnace, Journal of Process Control, 11 (2001) 565–586.

[75] S. Nag, V. Koranne, Development of material trajectory simulation model for blast furnace compact bell-less top, Ironmaking & Steelmaking, 36 (2009) 371-378.

[76] Z. Li, S. Kuang, S. Liu, J. Gan, X. Mao, Numerical investigation of burden distribution in ironmaking blast furnace, Powder Technology, 335 (2019) 385-397.

[77] H. Zhou, J. Wu, Z. Hong, L.P. Wang, S. Wu, M. Kou, G. Wang, Y. Luo, Numerical simulation of coke collapse and its optimization during burden charging at the top of bell-less blast furnace, Powder Technology, 389 (2021) 155-162.

[78] Z.Y. Zhou, H.P. Zhu, A.B. Yu, B. Wright, D. Pinson, P. Zulli, Discrete particle simulation of solid flow in a model blast furnace, Transactions of the Iron & Steel Institute of Japan, 45 (2005) 1828-1837.

[79] T. Ariyama, S. Natsui, T. Kon, S. Ueda, H. Nogami, Recent progress on advanced blast furnace mathematical model based on discrete method, ISIJ International, 19 (2014) 198-210.

[80] Y.W. Yu, H. Saxén, Experimental and DEM study of segregation of ternary size particles in a blast furnace top bunker model, Chemical Engineering Science, 65 (2010) 5237-5250.

[81] M. Akashi, H. Mio, A. Shimosaka, Y. Shirakawa, J. Hidaka, S. Nomura, Estimation of bulk density distribution in particle charging process using discrete element method considering particle shape, Transactions of the Iron & Steel Institute of Japan, 48 (2008) 1500-1506.

[82] H. Mio, M. Kadowaki, S. Matsuzaki, K. Kunitomo, Development of particle flow simulator in charging process of blast furnace by discrete element method, Minerals Engineering, 33 (2012) 27-33.

[83] Y.W. Yu, H. Saxén, Segregation behavior of particles in a top hopper of a blast furnace, Powder Technology, 262 (2014) 233-241.

[84] Mio, Narita, Nakano, Nomura, Validation of the burden distribution of the 1/3-scale of a blast furnace simulated by the discrete element method, Processes, 8 (2019) 6.

[85] H. Saxén, M. Nikus, On-line estimation of the ore-to-coke ratio in the blast furnace center, ISIJ International, 42 (2007) 115-117.

[86] K. Narita, S.I. Inaba, I. Kobayashi, K.I. Okimoto, M. Shimizu, K. Kuwano, K. Ikeda, Relationship of the gas temperature distribution with the descending rate and layer thickness of burden in the throat of blast furnace, Tetsu- to- Hagane, 65 (2010) 44-52.

[87] I. Morimasa, N. Kazuhiro, T. Kenji, S. Masayasu, O. Hajime, Influence of Ore/Coke Distribution on Descending and Melting Behavior of Burden in Blast Furnace, ISIJ International, 31 (1991) 505-514.

[88] Z. Li, S. Kuang, D. Yan, Numerical investigation of the Inner profiles of ironmaking blast Furnaces: effect of throat-to-belly diameter ratio, Metallurgical and Materials Transactions B, 48 (2017) 602-618.

[89] H. Mio, K. Yamamoto, A. Shimosaka, Y. Shirakawa, J. Hidaka, Modeling of solid particle flow in blast furnace considering actual operation by large-scale discrete element method, ISIJ International, 47 (2007) 1745-1752.

[90] Y.W. Yu, A. Westerlund, T. Paananen, H. Saxén, Inter-particle percolation segregation during burden descent in the blast furnace, Transactions of the Iron & Steel Institute of Japan, 51 (2011) 7.

[91] I. Ogata, M. Ichida, Expectation for coke quality seen from recent blast furnace operation in Japan, Tetsu-To-Hagane/Journal of the Iron and Steel Institute of Japan, 90 (2004) 600-608.

[92] M. Ichida, M. Takao, K. Kunitomo, S. Matsuzaki, T. Deno, K. Nishihara, Radial distribution of burden descent velocity near burden surface in blast furnace, ISIJ International, 36 (1996) 493-502.

[93] H.F. Li, H. Saxén, W.Q. Liu, Z.Y. Zou, L. Shao, Model-based analysis of factors affecting the burden layer structure in the blast furnace shaft, Metals - Open Access Metallurgy Journal, 9 (2019) 1003.

[94] F. Dong, C. Yan, C.Q. Zhou, Mathematical modeling of blast furnace burden distribution with non-uniform descending speed, Applied Mathematical Modelling, 39 (2015) 7554-7567.

[95] J.S. Chen, H.B. Zuo, Q.G. Xue, J.S. Wang, A review of burden distribution models of blast furnace, Powder Technology, 398 (2022) 117055.

[96] H. Nishio, T. Ariyama, Analysis on formation processes of burden distribution in blast furnace, Tetsu- to- Hagane, 68 (1982) 2330-2337.

[97] Y. Kajiwara, T. Jimbo, T. Sakai, Development of a simulation model for burden distribution at blast furnace top, Transactions of the Iron and Steel Institute of Japan, 23 (2006) 1045-1052.

[98] D.Y. E, Numerical investigation of mixed layer effect on permeability in a dynamic blast furnace, Engineering Reports, 2 (2020) 1-13.

[99] P. Cundall, O. Strack, A discrete numerical mode for granular assemblies, Géotechnique, 29 (1979) 47-65.

[100] S.B. Kuang, Z.Y. Li, A.B. Yu, Review on Modeling and Simulation of Blast Furnace, steel research international, 89 (2018) 1700071.

[101] E. Tsotsas, E.-U. Schlünder, Heat Transfer in Packed Beds with Fluid Flow: Remarks on the Meaning and the Calculation of a Heat Transfer Coefficient at the Wall, Chemical Engineering ence, 45 (1990) 819-837.

[102] T. Mitra, H. Saxén, Discrete element simulation of charging and mixed layer formation in the ironmaking blast furnace, Computational Particle Mechanics, 3 (2016) 541-555.

[103] Y.W. Yu, H. Saxén, Effect of DEM parameters on the simulated Iinter-particle percolation of pellets into coke during burden descent in the blast furnace, ISIJ International, 52 (2012) 788-796.

[104] M.Y. Kou, H. Zhou, S.L. Wu, Y.S. Shen, DEM simulation of cubical particle percolation in a packed bed, Powder Technology, 361 (2020) 306-314.

[105] Y.J. Jiang, X.Y. Fan, T.H. Li, S.Y. Xiao, Influence of particle-size segregation on the impact of dry granular flow, Powder Technology, 340 (2018) 39-51.

[106] S. Nag, S. Basu, A.B. Yu, A static approach towards coke collapse modelling in blast furnace, Ironmaking & Steelmaking, 36 (2009) 509-514.

[107] T. Mitra, H. Saxén, Investigation of coke collapse in the blast furnace using mathematical modeling and small scale experiments, ISIJ International, 56 (2016) 1570-1579.

[108] T. Mitra, H. Saxén, Simulation of burden distribution and charging in an ironmaking blast furnace, IFAC PapersOnLine, 48 (2015) 183-188.

[109] Y. Yang, K. Raipala, L. Holappa, Chapter 1.1 - Ironmaking, Treatise on Process Metallurgy, 2014.

[110] Q.F. Hou, D.Y. E, S.B. Kuang, Z.Y. Li, A.B. Yu, DEM-based virtual experimental blast furnace: A quasi-steady state model, Powder Technology, 314 (2017) 557-566.

[111] W.J. Yang, Z.Y. Zhou, A.B. Yu, Discrete particle simulation of solid flow in a three-dimensional blast furnace sector model, The Chemical Engineering Journal, 278 (2015) 339-352.

[112] F. Bambauer, S. Wirtz, V. Scherer, H. Bartusch, Transient DEM-CFD simulation of solid and fluid flow in a three dimensional blast furnace model, Powder Technology: An International Journal on the Science and Technology of Wet and Dry Particulate Systems, 334 (2018) 53-64.

[113] Z.Y. Zhou, H.P. Zhu, A.B. Yu, P. Zulli, Numerical Investigation of the Transient Multiphase Flow in an Ironmaking Blast Furnace, Transactions of the Iron & Steel Institute of Japan, 50 (2010) 515-523.

[114] C. Goniva, C. Kloss, A. Hager, S. Pirker, An open source CFD-DEM perspective, proc openfoam workshop, (2010).

[115] J. Ai, J.F. Chen, J.M. Rotter, J.Y. Ooi, Assessment of rolling resistance models in discrete element simulations, Powder Technology, 206 (2011) 269-282.

[116] H. Hertz, Ueber die Berührung fester elastischer Körper, 1882 (1882) 156-171.

[117] A. Di Renzo, F.P. Di Maio, An improved integral non-linear model for the contact of particles in distinct element simulations, Chemical Engineering Science, 60 (2005) 1303-1312.

[118] Y. Tsuji, T. Tanaka, T. Ishida, Lagrangian numerical simulation of plug flow of cohesionless particles in a horizontal pipe, Powder Technology, 71 (1992) 239-250.

[119] G.M. Hu, Z.Y. Hu, B. Jian, L.P. liu, H. Wan, On the Determination of the Damping Coefficient of Non-linear Spring-dashpot System to Model Hertz Contact for Simulation by Discrete Element Method, 2010 WASE International Conference on Information Engineering, 3 (2010) 295-298.

[120] J. Ai, J.F. Chen, J.M. Rotter, Y.O. Jin, Assessment of rolling resistance models in discrete element simulations, Powder Technology, 206 (2011) 269-282.

[121] M. Michele, S.E. Hugh, Discrete Element Method (DEM) for Industrial Applications: Comments on Calibration and Validation for the Modelling of Cylindrical Pellets, Kona, 32 (2015) 236-252.

[122] Z.P. Zhang, L.F. Liu, Y.D. Yuan, A.B. Yu, A simulation study of the effects of dynamic variables on the packing of spheres, Powder Technology, 116 (2001) 23-32.

[123] C.J. Coetzee, Review: Calibration of the discrete element method, Powder Technology, 310 (2017) 104-142.

[124] C.Z. Li, T. Honeyands, D. O'Dea, R. Moreno-Atanasio, The angle of repose and size segregation of iron ore granules: DEM analysis and experimental investigation, Powder Technology, 320 (2017) 257-272.

[125] G.K.P. Barrios, R.M. De Carvalho, A. Kwade, L.M. Tavares, Contact parameter estimation for DEM simulation of iron ore pellet handling, Powder Technology, 248 (2013) 84-93.

[126] L.M. Tavares, R.P. King, Single-particle fracture under impact loading, International Journal of Mineral Processing, 54 (1998) 1-28.

[127] B.K. Mishra, C. Murty, On the determination of contact parameters for realistic DEM simulations of ball mills, Powder Technology, 115 (2001) 290-297.

[128] S. Rosenkranz, S. Breitung-Faes, A. Kwade, Experimental investigations and modelling of the ball motion in planetary ball mills, Powder Technology, 212 (2011) 224-230.

[129] L. Wang, B. Wu, Z. Wu, L. Rui, F. Xin, Experimental determination of the coefficient of restitution of particle-particle collision for frozen maize grains, Powder Technology, 338 (2018) 263-273.

[130] K. Zhang, W.D. Yu, D. Li, D.F. Zou, S.Y. Zhang, Measurement and simulation validation of numerical model parameters of fresh concrete, Science and Engineering of Composite Materials, 28 (2021) 437-452.

[131] A. Agarwal, A. Tripathi, A. Tripathi, V. Kumar, A. Chakrabarty, S. Nag, Rolling friction measurement of slightly non-spherical particles using direct experiments and image analysis, Granular Matter, 23 (2021) 60.

[132] A.H. Madadi Najafabadi, A. Masoumi, S.M. Vaez Allaei, Analysis of abrasive damage of iron ore pellets, Powder Technology, 331 (2018) 20-27.

[133] S.Y. Wei, H. Wei, H. Saxén, Y.W. Yu, Numerical analysis of the relationship between friction coefficient and repose angle of blast furnace raw materials by Discrete Element Method, Materials, 15 (2022) 903.

[134] C.M. Wensrich, A. Katterfeld, Rolling friction as a technique for modelling particle shape in DEM, Powder Technology, 217 (2012) 409-417.

[135] R.P. Zou, A.B. Yu, Evaluation of the packing characteristics of mono-sized non-spherical particles, Powder Technology, 88 (1996) 71-79.